NUMERICAL STUDY ON GASOLINE DIRECT INJECTION SPRAYS

A Thesis Submitted to
the Graduate School of Engineering and Sciences of
İzmir Institute of Technology
in Partial Fulfillment of the Requirements for the Degree of

MASTER OF SCIENCE

in Energy Engineering

by
Yagmur GULEC

December 2015
IZMIR

We approve the thesis of **Yagmur GULEC**

Examining Committee Members:

Ass. Prof. Dr. Alvaro DIEZ
Mechanical Engineering
Izmir Institute of Technology

Ass. Prof. Dr. Turhan COBAN
Mechanical Engineering
Ege University

Ass. Prof. Dr.Onursal ONEN
Mechanical Engineering
Izmir Institute of Technology

23 December 2015

Ass. Prof. Dr. Alvaro DIEZ
Supervisor, Department of Electrical and Electronics Engineering
Mechanical Engineering
Izmir Institute of Technology

Prof. Dr. Gulden Gokcen AKKURT
Head of the Department of
Energy Engineering

Prof. Dr. Bilge KARACALI
Dean of the Graduate School of
Engineering and Sciences

ACKNOWLEDGMENTS

I would like to thank to Ass. Prof. Dr Alvaro DIEZ and Ass. Prof. Dr. Unver OZKOL for their contributions. I also would like to thank to my dear grandmother, mother, sister and aunt. They always support and help me throughout my lifetime.

ABSTRACT

NUMERICAL STUDY ON GASOLINE DIRECT INJECTION SPRAYS

Gasoline direct injection technology is a combination of the advantages of diesel engine and spark ignition engines. Hence, the gasoline fuel is injected directly to combustion chamber. It provides finer atomization to allow evaporation more rapidly than traditional gasoline engines and less emissions in terms of NO_x and particulate than diesel engines. The understanding of spray behaviour is a significant point to control optimal air/fuel mixture and misfiring.

This thesis presents a numerical investigation of a GDI injector under flash and non-flash boiling conditions. The study is performed with sprays injected into a constant volume chamber. The purpose of the thesis is to develop a CFD model to compare it with experimental spray penetration and spray angle results. Firstly, the model is validated in terms of spray penetration. Secondly, the model is applied to nine different conditions including flash and non-flash boiling conditions. The spray penetration and angle comparisons between numerical and experimental results were done.

ÖZET

BENZİN DİREK ENJEKSİYON SPREYLERİ ÜZERİNE NÜMERİK ÇALIŞMA

Benzin direk enjeksiyon teknolojisi, dizel enjeksiyon ile benzin motorlarının avantajlarının bir kombinasyonudur. Benzin direk motorlarında direk olarak benzin yanma odasına püskürtülür. Bu hem daha küçük damlacıklara ayrılmasına bu sayede hızlıca buharlaşmasına ve dizel motorlara gore NO_x ve katı madde emisyonlarının daha az olmasına olanak sağlar. Spreyin davranışını anlamak optimum yakıt-hava karışımı açısından önemlidir.

Bu tez, direk benzin enjektör spreylerinin flash boiling ve olmayan koşullardaki nümerik çalışmasını sunmaktadır. Bu tezin amacı, deneysel sprey penetrasyonu ve sprey açısı sonuçlarıyla kıyaslama yapabilmek için bir CFD model geliştirmeyi amaçlamaktadır. Öncelikle model sprey penetrasyonu ile doğrulandı. Daha sonra, modelde flash ve flash boiling olmayan koşulları içeren dokuz farklı işletme koşulları uygulandı. Nümerik ve deneysel sprey açısı ve sprey penetrasyon sonuçları karşılaştırıldı.

TABLE OF CONTENTS

LIST OF FIGURES

LIST OF TABLES

LIST OF SYMBOLS

We ..... Weber number
Re ..... Reynolds number
Z ..... Ohnesorge number
D ..... nozzle diameter
σ ..... surface Tension
ρ_l ..... density of Liquid
μ_l ..... dynamic Viscosity of Liquid
u_{rel} ..... relative velocity between droplet and gas
C_d ..... discharge coefficient
L_A ..... characteristic atomization length scale
τ_A ..... characteristic atomization time scale
F_D ..... drag force
C_D ..... drag coefficent
h_v ..... vapor enthalpy
h_d ..... liquid enthalpy
R_0 ..... universal gas constant
r_c ..... compression ratio
V_c ..... clearance Volume
T_f ..... fuel temperature
P_v ..... chamber pressure

LIST OF ABBREVIATIONS

IMEP . . . . . indicated mean effective pressure
BSFC . . . . . brake-specific fuel consumption
PISO . . . . . pressure-implicit split operator
SIMPLE . . . . . Semi-Implicit Method for Pressure Linked Equations
SI . . . . . spark ignition
CI . . . . . compression ignition
SOI . . . . . start of injection
mep . . . . . mean effective pressure
NO_x . . . . . oxides of nitrogen
TAB . . . . . Taylor-analogy breakup model
PDF . . . . . probability density function

CHAPTER 1

INTRODUCTION

Regulations in terms of pollutant emissions are getting stringent. This pushes researchers in automotive field to develop an engine that provides more fuel economy, namely enhanced brake-specific fuel consumption. Diesel engines offers fuel economy and performance. However, they have higher noise levels, a more limited speed range, lower startability, higher particulate and NO_x emissions. In addition, they require higher injection pressure and more complicated and expensive after-treatment devices to meet future emission legislations. Gasoline direct injection (GDI) concept has bridged the gap between Spark-ignition engines and diesel engines. Direct injection (DI) gasoline engines have the potential to realise the higher specific power output and improve fuel economy due to their ability to minimise knocking combustion at full load operations and reduce pumping losses at part load conditions. To control mixture formation in engines, the spray characteristic should be understood. Beside of experimental studies of spray structure, numerical models have been developed to validate with experimental data. Instead of costly repetitive experimental works, more advances in terms of ability to predict the spray pattern better are being developed.

1.1. Background and Motivation

High injection pressures promotes vaporization and atomization. However, it could cause over penetration wall or piston wetting resulting in high level of hydrocarbon and soot emissions. When fuel undergoes a flash boiling condition, spray gets wider and penetrates shorter distance from nozzle. This transformation can be taken advantage in terms of better atomization and shorter penetration. That is why researchers have been focusing flash boiling phenomenon. In this study, spray penetration and angle under flash and non-flash boiling conditions was numerically investigated.

1.2. Outline of The Thesis

Some theoretical background about internal combustion engines and engine spray structure are mentioned in Chapter 2. This chapter gives brief information about Diesel injection, GDI technology and its stratified charge concepts. Primary and secondary breakup phenomena is summarised and previous studies on numerical simulations are focused in this chapter. In Chapter 3 representative differential equations for liquid and gas phase and coupling source terms of both phases are denoted with turbulence model used. In addition to them plain orifice atomizer and effervescent atomizer models for primary breakup simulation and WAVE breakup model for secondary breakup of droplets are given information. And then domain and boundary conditions are shown. Numerical settings such as initial conditions and grid and time-step resolutions are reported with validation in this chapter. Chapter 4 represents the numerical results in terms of spray angle and penetration for each operating conditions. The comparison of the results and their agreement with the experimental data are discussed. The reasons why they do not match the experimental data are stated. In addition to Chapter 4 the improvements on the model to predict better the spray behaviour are highlighted in Chapter 5. The implementation of some phenomenological approaches to avoid non-physical coupling between the two phases is also explained.

CHAPTER 2

LITERATURE SURVEY

In this chapter firstly internal combustion engines and fuel injection systems are introduced and then spray formation in a combustion chamber is explained briefly.

2.1. Introduction to Internal Combustion Engines

Internal combustion engines convert thermal energy released due to fuel combustion into mechanical energy. Thus the thermal efficiency of a device that uses thermal energy such as internal combustion engines could be performance criteria. While Otto cycle is used in spark ignition injection engines, Diesel cycle is the working principle for compression ignition engines.

For Otto cycle, the thermal efficiency can be formulated as below,

$$\eta_{th} = 1 - \frac{1}{r^{\gamma-1}}, \tag{2.1}$$

where γ is the specific heat ratio that varies with the fuel for air/fuel mixture and is generally close to the air value of 1.4, and r_c is the compression ratio which is the ratio of maximum cylinder volume to minimum cylinder volume. It is clear from Eq. 2.1 the thermal efficiency increases with the compression ratio. On the other hand the uncontrolled combustion, known as knocking readily affected by compression temperature of air-fuel mixture limits the compression ratio. Injection systems have been pushed to be developed by the need of higher efficiencies without knocking. The injection system have been evolved from port fuel injection to direct injection to directly control air-fuel mixture formation. Direct injection of liquid fuel allows the fuel evaporation to take heat from the surrounding air and bring about the air temperature to drop. With the charge cooling effect of direct injection, higher pressure can be employed without the risk of knocking. The compression ratio is allowed to increase by 1 and 1.5 units. (Baumgarten, 2006).

To mention about the main areas to be developed in gasoline engines, one of these areas is minimisation of pumping losses due to partly open throttle valve to meter air mass flow rate at especially part load conditions (see Fig. 2.1). In fuel injection systems there is no valve to block air entrance so that maximum appropriate quantity of air can be introduced into the chamber, the fuel quantity is controlled depending on engine load. The

injection techniques for gasoline engines can be divided into two main categories; port fuel injection and direct injection. Port fuel injection has also two main categories which is single-point injection and multi-point injection. This two main categories differ at the point where the fuel is injected. In single-point injection systems carburetors are replaced by a central injection unit. There are two types of injection systems in gasoline-powered vehicles-port injection and direct injection. Both systems use computer-controlled electric injectors to spray fuel into the engine, but the difference is where they spray the fuel. Port injection sprays the fuel into the intake ports where it mixes with the incoming air.

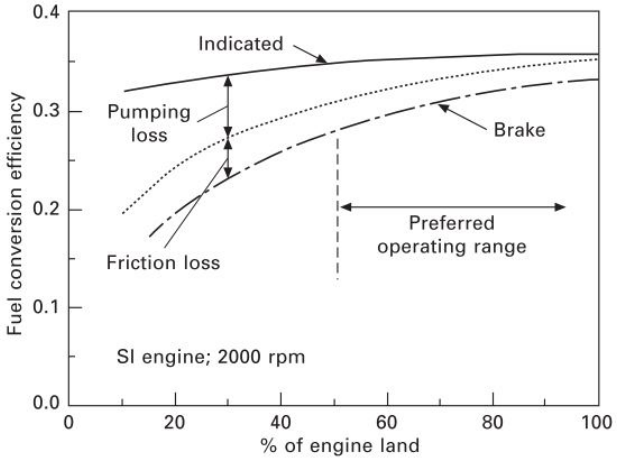

Figure 2.1. Gasoline engine pump losses (Horrocks, 2010)

2.1.1. Port Fuel Injection

In single-point injection, which can be defined as a bridge between the carburetors and multipoint injection, the carburetor is replaced by a central injection unit. The prepared fuel mixture is introduced into the cylinder via the intake manifold.In this kind of injection there is one injection point upstream the intake manifold. Depending on the design of the intake manifold, whereas the cylinder closest to the intake manifold gets a bit too much fuel, the cylinder farthest runs in lean mode. As opposed to the single-point injection, multipoint injection means there is a separate fuel injector for each cylinder so that this inconsistency of the amount of fuel between the cylinders could be avoided. Thus multipoint inject improved the power generation and reduced wasted fuel (see the Fig. 2.2). Moving the injector into the combustion chamber has been a jump so-called

direct injection from multipoint injection systems.

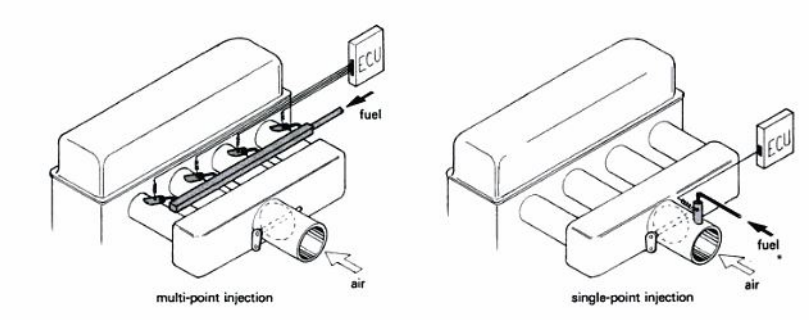

Figure 2.2. Single Point and Multipoint Injection (Hillier and Coombes, 2004)

2.1.2. Direct Injection Systems

By placing the injector inside the cylinder, the control over the amount of fuel gains much precision, which results in better fuel economy and optimized air/fuel mixture for cleaner burning. Direct injection supply high degree atomization atomization to allow the fuel evaporation in a short time. While diesel injection pressures varies between 100 and 200 MPa, the maximum injection pressures are limited to approximately 25 MPa to avoid the pump wear since gasoline does not serve as a lubricant as well as diesel does. There are two main groups belonging to high-pressure injection systems; common rail and unit systems.

In common rail injection, a high-pressure pump stores a reservoir of fuel at high pressure and continuously feeds the rail (see Fig. 2.3). Needle movements, which allows the fuel to go out of the injector, and thus injection timing and duration are controlled by solenoid or piezoelectric valves. For the reason that this control is independent of pressure generation, the common rail injection system is able to keep the injection event at the desired settings.

Unit injectors are the second group of the direct injectors. In contrast to the common rail systems, the injection pressure generation and injection event occurs dependently on each other.

Fig. 2.4 shows unit injector during both positions closed and open. Once the solenoid valve is opened, excess fuel is discharged. When the start of injection is needed, the solenoid is closed and the plunger compress the fuel so that the pressure can lift the needle, and injection begins (Fig. 2.4). To compare injection profiles of a common rail

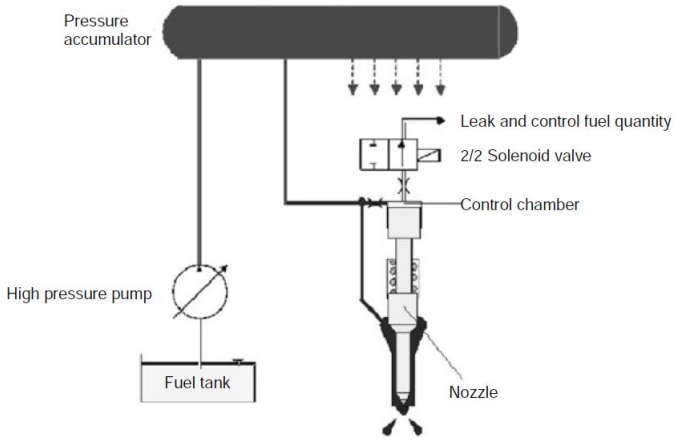

Figure 2.3. Common rail injection systems (Johnson et al., 2010)

injector and unit injector, whereas unit injector is triangular due to large feed rate of the plunger, a common rail injector is rectangular with an almost constant profile for a desired time (Fig.2.5).

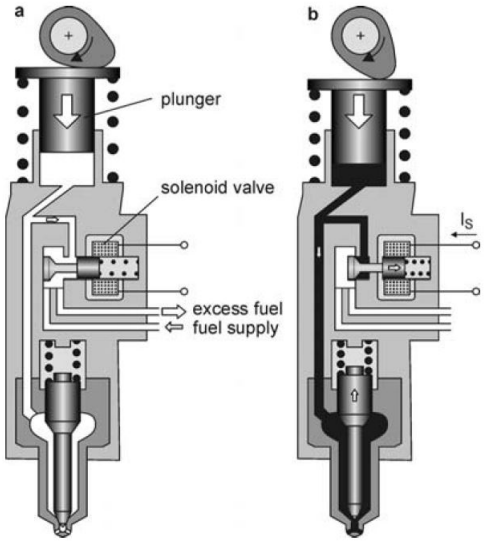

Figure 2.4. Schematic illustration of control of a unit injector (Baumgarten, 2006)

In diesel injectors, there are two types of nozzles which are the most important part of the injectors: the sac hole nozzle and the valve covered orifice nozzle (VCO), see Fig. 2.6. It is noticed that in sac hole nozzle the volume below the needle seat of the sac hole is larger than VCO nozzle has. The volume must be kept as small as possible otherwise the liquid can enter into combustion chamber after the end of injection and can result in late evaporation causing hydrocarbon emission and bad dispersion. In terms of

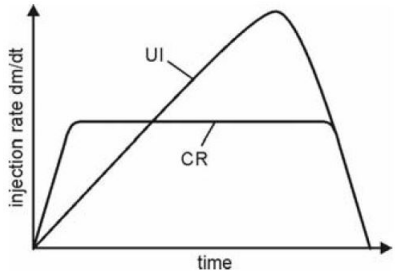

Figure 2.5. Injection rate profiles of a common rail injector and a unit injector (Baumgarten, 2006)

emissions VCO is more advantageous.

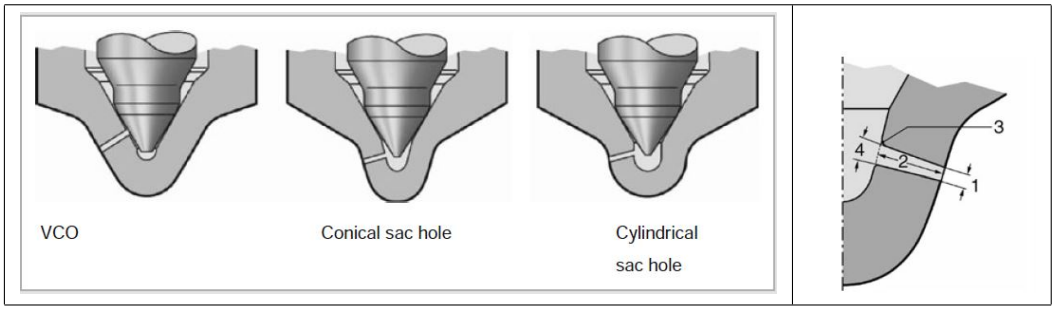

Figure 2.6. Nozzle Types and Nozzle Geometry 1-Nozzle diameter 2-Nozzle length (Johnson et al., 2010)

2.2. Introduction to Gasoline Direct Injection Engines (GDI)

Diesel engines offer excellent efficiency but suffer from soot and NO_x emissions. Regarding the fulfilment of future legistations of NO_x and soot emissions, while diesel engine require more expensive after-treatment devices, the conventional port fuel injection gasoline engine can meet these legistations with a conventional three-way catalyst system for exhaust gas aftertreatment.

Gasoline direct injection engines offer two main operating modes: stratified and homogeneous mode (see Fig. 2.7). In full load conditions the injection is applied in the intake stroke, which is earlier than the one for stratified mode so that the necessary amount of fuel is injected and the fuel have enough time to form a homogeneous stoichiometric mixture with air charge. There is a transition mode so-called homogeneous lean mode in

which the large amount of fuel is injected early during the intake stroke so the mixture is homogeneous but lean and the rest of the fuel is injected in the compression stroke from stratified to homogeneous mode. In Fig. 2.1 has illustrated that pump losses at part load creates inefficiency and thus much fuel consumption in PFI gasoline engines and part load conditions should be investigated to improve in terms of fuel consumption. Hence, stratified charge mode in GDI offers the fuel economy and less emissions. There are three possible concepts for stratified mode shown in Fig. 2.8.

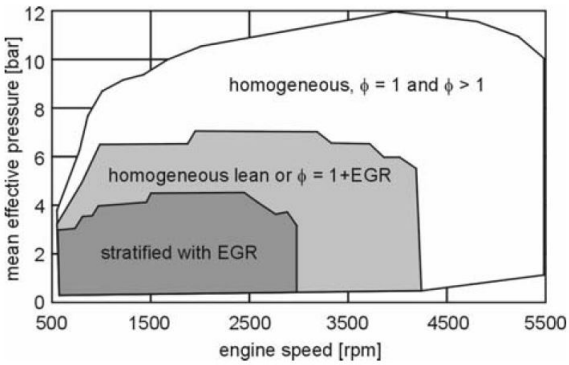

Figure 2.7. Operating Modes for GDI (Baumgarten, 2006)

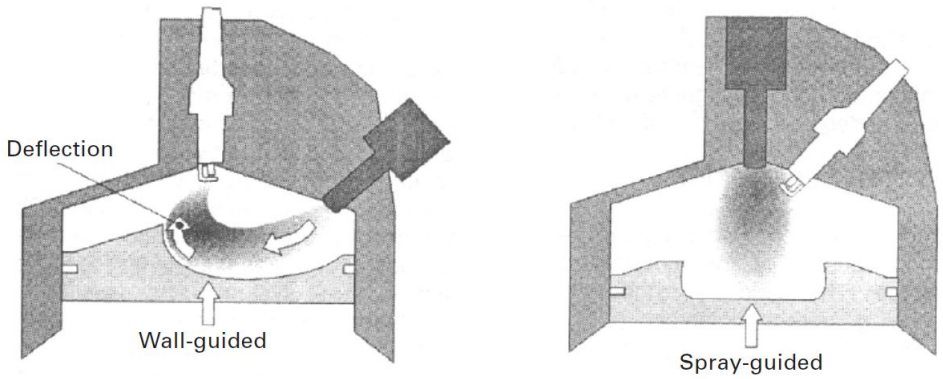

Figure 2.8. Possible stratified modes concepts (Horrocks, 2010)

In wall guided systems a great amount of fuel is injected onto the wall and can not thoroughly evaporate, resulting in a unburned hydrocarbons and CO. However, this concept provides powerful combustion and prevents misfiring. Moreover, a stable air motion in the air guided concept keeps the spray plume more compact, assist the spray to mix with air homogeneously and carries the spray to the spark plug. The combination of air

and wall guided techniques provides a stable stratified charge and is today's trend in GDI engines. Besides, the spray guided techniques distinguish as a characteristic of closeness in placement of the injector and the spark plug. The spray is directed to the spark plug by its own energy and thus strong air motions are not necessary and they even disturbs while the spray is being transported. Since the injector and the spark plug are close to each other, the injection duration is very short, which requires higher injection pressures for mixture formation. In contrast to two other concepts the control of optimal conditions are achieved more easily and are dependent on injection timing. The spray guided concept is promising in terms of thermodynamically optimal timing and fuel economy at part load. However, there are two main problems in this concept. First, the formation of extremely compact and well-mixed spray with high stratification in a very short time must be obtained and at the same time soot emissions, must be avoided and unburned hydrocarbons. The ignitable fuel-air mixture at the spark plug requires optimal placements of injector and spark plug. A small displacement causes misfiring and deposition of of liquid fuel on the spark plug, if liquid fuel wets the spark plug, this may result in soot emission and carbonization causing extreme thermal stresses on the spark plug. In-cylinder pressure influences the spray characteristics, which is hard to rely on ignition at different load points. In other words, the more the injection timing is retarded, the higher the pressure inside the cylinder is getting during injection. This will result in changes in spray shape. To solve this problem an injector which keep spray independent of pressure has to be developed. A future possible ignition technique is laser-induced technique which can focus on the spatial position before spray shape is influenced by backpressure (Baumgarten, 2006).

2.3. Engine Spray Structures

2.3.1. Full-Cone Spray

The injector type used in this investigation is a single-hole injector. This kind of injector creates full-cone sprays. In Fig. 2.9 the structure of a full-cone spray is depicted. Injected fuel at high pressure breaks up in consequence of cavitation and turbulence in nozzle and takes the conical shape. Due to this primary breakup in dense region near the nozzle large ligaments are formed whereas in dispersed regions the droplets take shape. The following break-up process of already existing droplets into smaller ones is called

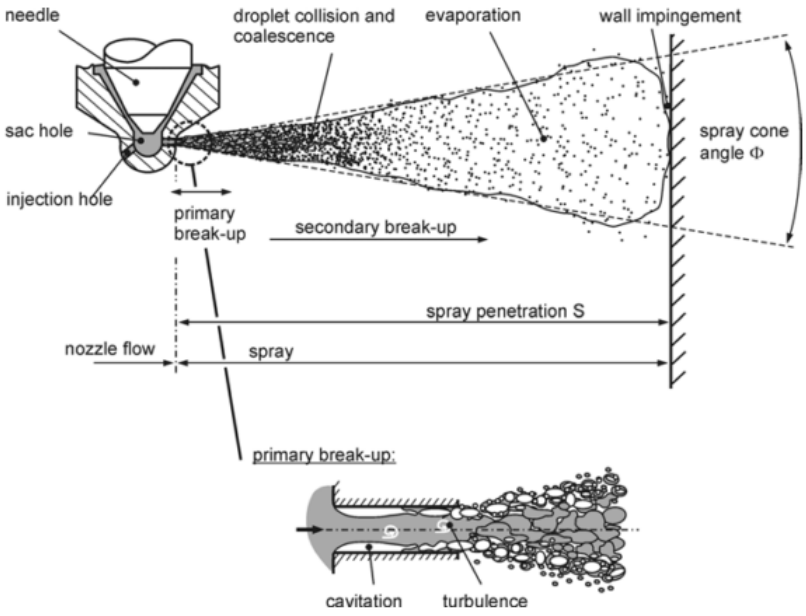

Figure 2.9. Break-up of a full-cone spray in engine (Baumgarten (2006))

secondary break-up and is caused by aerodynamic forces due to the relative velocity between droplets and surrounding gas.

The drops at the spray tip undergo the strongest drag force and are much more decelerated than the droplets that follow them since the aerodynamic force decelerate the droplets. Hence, the droplets at the spray tip are continuously are replaced by new ones and new ones push the droplets with low kinetic energy towards the outer region of spray. Liquid mass mostly occupies the regions near the spray axis while relatively less liquid mass and more fuel vapour possess the outer regions. In addition the fraction of fuel decreases downstream the nozzle as the mixture entrains with the surrounding air.

The behaviour of the full cone sprays can be described by some parameters such as spray penetration, spray cone angle, average droplet diameter and break-up length. Hiroyasu and Arai (1990) developed the spray penetration and spray cone angle formulation. According to them the spray penetration length can be investigated by dividing into two phases. For the first phase that is the duration from the beginning of injection $(t = 0)$ to the moment when the liquid undergoes the primary break-up, Eq. 2.2 is valid and linear growth of the spray penetration is seen. During the second phase $(t > t_{break})$ in which the spray tip velocity is smaller than the phase Eq. 2.3 is used. As a criteria for dividing the phases the break-up time is computed via Eq. 2.4.

$$t < t_{break} : S = 0.39(\frac{2\Delta P}{\rho_l})^{0.5}t \tag{2.2}$$

$$t > t_{break} : S = 2.95(\frac{\Delta P}{\rho_g})^{0.25}(Dt)^{0.5} \tag{2.3}$$

$$t_{break} = \frac{28.65\rho_l D}{(\rho_g \Delta P)^{0.5}} \tag{2.4}$$

where D is nozzle diameter, $\Delta P = P_{inj} - P_{chamber}$ is the pressure difference.
Sauter Mean Diameter (SMD) is used to describe as a average model drop whose volume-to-surface ratio equals to the ratio of the sum of all droplet volumes in the spray to the sum of all droplet surface areas (see Eq. 2.5).

$$SMD = \frac{\sum_{i=1}^{n} d_i^3}{\sum_{i=1}^{n} d_i^2} \tag{2.5}$$

For more effective evaporation and mixture formation more surface area, in other words smaller SMD, is a necessity. Hiroyasu et al. (1989) and Hiroyasu and Arai (1990) improved empirically a mathematical formulation (Eq. 2.6) associating Sauter Mean Diameter to We and Re numbers.

$$\frac{SMD}{D} = 0.38Re^{0.25}We^{-0.32}\left(\frac{\mu_l}{\mu_g}\right)^{0.37}\left(\frac{\rho_l}{\rho_g}\right)^{-0.47} \tag{2.6}$$

Liquid core length consisting of very dense cluster of ligaments and drops is hard to observe empirically. However, some authors developed a formulation of the liquid core length. Chehroudi et al. (1985) proposed the model (Eq. 2.7) via the electrical resistance measurements in the core region. In addition to the model of Chehroudi et al. (1985), Hiroyasu and Arai (1990) gave more detailed expression.

$$L_C = C.D.\sqrt{\frac{\rho_l}{\rho_g}} \tag{2.7}$$

where C is a constant depending on nozzle flow conditions.

$$L_b = 7.D.\left(1 + 0.4\frac{r}{D}\right).\left(\frac{P_g}{\rho_l u^2}\right)^{0.5}\left(\frac{L}{D}\right)^{0.13}.\left(\frac{\rho_l}{\rho_g}\right)^{0.5} \tag{2.8}$$

where r is the radius of the inlet edge of the hole.

2.4. Break-up Regimes of Liquid Jets

The break-up of a liquid jet is governed by different break-up mechanism, depending on the relative velocity and the properties of the liquid and surrounding gas. The distance between the nozzle and the point of first droplet formation, the so-called break-up length, and the size of product droplets distinguish these different mechanisms

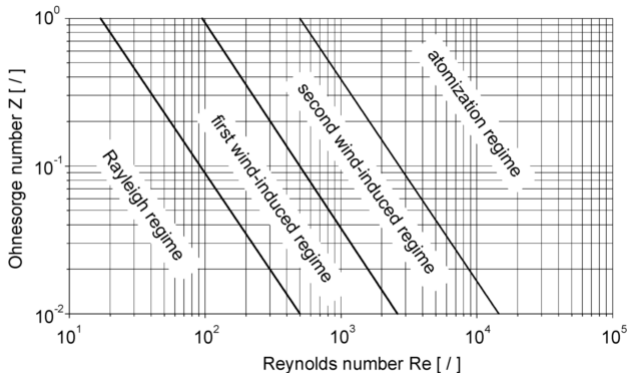

Figure 2.10. Ohnesorge diagram:jet break-up regimes (Baumgarten (2006))

(Baumgarten (2006)). A schematic description of the different jet break-up regimes is given in Fig. 2.10.

$$We_l = \frac{u^2 D \rho_l}{\sigma} \tag{2.9}$$

$$Re = \frac{u D \rho_l}{\mu_l} \tag{2.10}$$

Eliminating the jet velocity u, Ohnesorge derived the dimensionless Ohnesorge number (Z),

$$Z = \frac{\sqrt{We_l}}{Re} = \frac{\mu_l}{\sqrt{\sigma \rho_l D}} \tag{2.11}$$

which includes all relevant fluid properties as well as nozzle diameter D. Fig. 2.10 shows the Ohnesorge diagram, in which Z is given as a function of Re. The only variable is the liquid velocity u as long as the nozzle geometry is fixed and the liquid properties are not varied. The graph in Fig. 2.11 represents all break-up regimes depending on velocity and the function of break-up length according to jet fluid velocity u. The theoretical

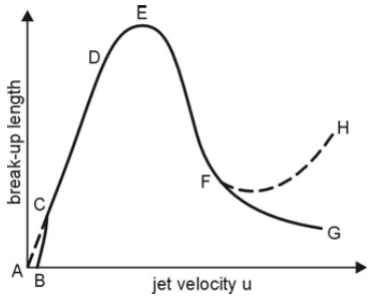

Figure 2.11. Jet surface break-up length (Baumgarten (2006))

description of jet break-up in the atomization regime is much more complex than in any

other regime, because the disintegration process strongly depends on the flow conditions inside the nozzle hole, which are usually unknown and of a chaotic nature (Baumgarten (2006)).

2.5. Break-Up Regimes of Liquid Drops

Aerodynamic forces (friction and pressure) induced by u_{rel} between droplet and surrounding gas cause the break-up of drops in a spray, which in turn the child droplets are again subject to further break-up. The aerodynamic forces result in an unstable growing of waves on the gas/liquid interface or of the whole droplet itself, which finally leads to disintegration and to the formation of smaller droplets. Surface tension force mitigates the effect of the deformation forces, trying to keep the droplets spherical. Depending on the curvature of the surface, the surface tension force increase as well as critical relative velocity as the droplets gets smaller, which conduct an instable droplet deformation and to disintegration (Baumgarten (2006)). This can be explained by the gas phase Weber number (Eq. 2.12).

$$We_g = \frac{u_{rel}^2 d \rho_g}{\sigma} \tag{2.12}$$

where d is the droplet diameter before break-up.

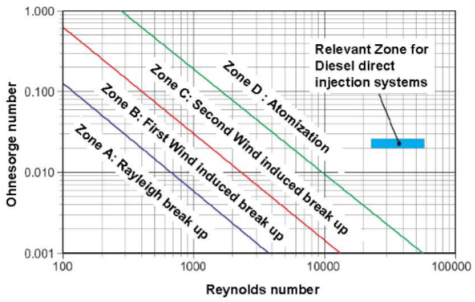

Figure 2.12. Drop break-up regimes (Bekdemir et al. (2008))

Fig. 2.13 state pertinent mechanisms of drop break-up, which depends on We number. From the point of sprays in engine of view, most of disintegration occurs near the nozzle at high We numbers, while further downstream, the We numbers considerably decrease due to reduced droplet diameters as a consequence of evaporation and previous break-up and due to a reduction of the relative velocity caused by drag forces.

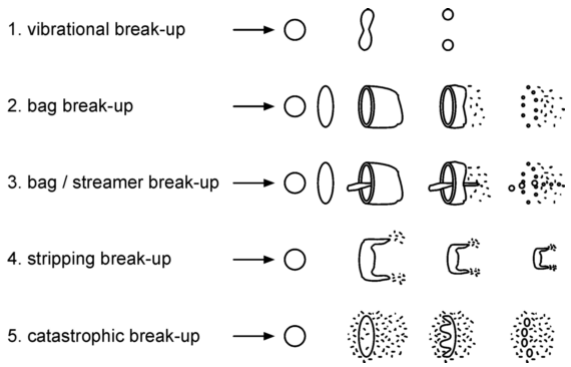

Figure 2.13. Atomization regimes (Baumgarten (2006))

2.6. Previous Studies on Numerical Simulations

Some researchers concentrated on momentum flux to validate their CFD model. Postrioti et al. (2009) prepared transient CFD model of diesel spray as a impacting jet on a target and compared between the measured time-varying global momentum flux results which the impact force on the target of the momentum test rig at a specified distance from nozzle and the numerical result. In addition to this study, Postrioti and Battistoni (2010) added free jet configuration and derived momentum balance equation for total resulting force evaluation at a specified distance for the free jet case to compare with the same global momentum flux data. Both studies were related to the global momentum flux, Postrioti et al. (2011) developed local spray measurement test bench and measured spatial momentum flux distributions. The integration of either experimental local momentum flux or numerical local momentum flux gave satisfying results when comparing with the global momentum flux result for each of them. The comparison with CFD free jet case was done in terms of local momentum flux distributions.

Moreover, some research groups focused on spray penetration and spray angle for CFD validation rather than momentum flux. Bekdemir et al. (2008) used Fluent software with diesel injection at 800 bar and took into account breakup, variations in droplet shape by dynamic drag model and droplet collisions. The model was supported by phenomenological spray model (Versaevel et al., 2000) to avoid convergence problems. The comparison were done with spray penetration with evaporating and non-reacting case and added combustion case.

Coupling of two-phases can have problems since the exchange of mass, momentum and energy are strongly mesh dependent. Some researchers developed some ap-

proaches to avoid mesh dependency. In the new spray model of Abani et al. (2008) the components of gas velocity were calculated from gas jet theory to avoid errors in predicting the droplet-gas relative velocity and droplet-droplet collisions which are the main sources of mesh-dependency. Comparing their results with experimental data in terms of SMD, spray tip penetration with different grid size configurations, they validated the model. The model substantially prevented grid dependency since the Lagrangian-Eulerian methods were shown strongly mesh-dependent (Abraham, 1997). However this study was available for steady state injection profiles. Since in real engine conditions injection is time-varying, they extended the model for unsteady in-cylinder conditions (Abani et al., 2008). Kösters and Karlsson (2011) developed a new spray model called VSB2 which differs from traditional Lagrangian methods that the parcel containing exactly alike droplets were replaced by irregular blob of a certain size distribution. This method was less grid dependent since stochastic blobs interact with only surrounding bubbles (see Fig. 2.14). Firstly, they employed their model with either high or low pressure configurations, compared standard k-ε and RNG k-ε and tuned k-ε constants.They researched grid sensitivity comparing the vapour and liquid penetration results with the experimental results and even the injector position. Some phenomenological approaches and models help researchers

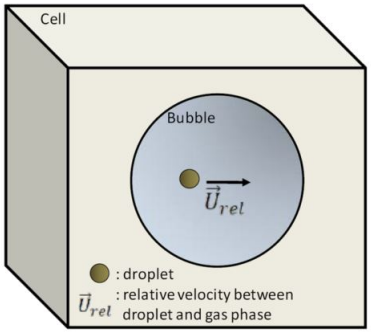

Figure 2.14. Definition of VSB2 (Kösters and Karlsson (2011))

when some assumptions needs to be done regarding initial diameter. Badami et al. (2008) used one of the proposed phenomenological model of Hiroyasu et al. (1989) for initial droplet diameter size and SMD. In this study the drag coefficient is modified from spray penetration formula divided into two phases prior to primary breakup and after primary in time the study of Hiroyasu and Arai (1980) to control the spray penetration. Hence, the spray follows the tip without needing additional momentum source.

Already proposed break-up models can be applied accordingly to the phases of injection duration. Since WAVE (Reitz and Diwakar, 1987) and TAB (O'Rourke and Ams-

den, 1987) model do not take into account the fluid conditions inside the nozzle on spray dynamics, the cavitation-induced model of Arcoumanis et al. (1997) and the turbulence-induced model of Huh and Gosman (1991) were developed. Bianchi and Pelloni (1999) used (Huh and Gosman, 1991) model for primary breakup while the secondary break up was modeled by TAB model. Bianchi et al. (2001) updated the treatment of the spray breakup in the early period of injection in the hybrid model of Bianchi and Pelloni (1999) by changing the treatment into TAB model. They validated their model with spray penetration, SMD and cone angle.

2.7. Flash-Boiling

When superheated liquid in terms of discharge pressure exits nozzle, it undergoes a sudden drop in pressure, which is the metastable state. Bubbles form inside the liquid and use up the latent heat of the fluid so that the fluid temperature drops. This drop continues until the saturation temperature at ambient pressure is reached while bubbles are growing. The flash-boiling process has three stages: nucleation, vapour bubbles growth and atomization whose mechanisms are discussed in the literature: bubble coalescence, inertial shattering, and micro explosions.

Flashing can be useful or disturbing depending on the applications. In some systems, flashing causes to reduce droplet sizes and these small droplets evaporates quickly. These thermodynamic conditions can occur in part load conditions for GDI engines. This can be useful for more efficient combustion. On the other hand, the reduction of the droplet sizes results in reduction of inertia of the droplets and thus reduction of the penetration of the fuel. Under flash boiling conditions in some experimental works it is shown that the spray shape dramatically changes.

In Fig. 2.15 the disintegration changes as the temperature is raised above the boiling point. The jet cone angle increases by increasing the temperature.

Xu et al. (2013) reported AtSPR (Air to Saturation Pressure Ratio) to explain the tendency to flash boiling (Table 2.1).

Table 2.1. AtSPR Ranges

AtSPR>1	No flash boiling
$0.3 <$ AtSPR < 1	Transition Zone
AtSPR<0.3	Full Flash-Boiling

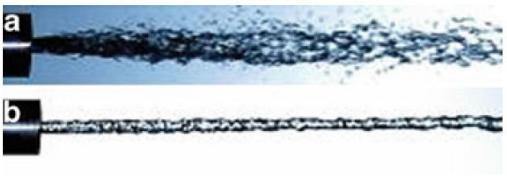

Figure 2.15. (a)The temperature is above the boiling point. (b) The temperature is below the boiling point. (Ashgriz (2011))

Postrioti et al. (2015) performed momentum flux experimental study to understand the behaviour of spray under flash boiling and non-flash boiling conditions. In flash-boiling conditions (Air to Saturation Pressure Ratio below 0.3) the spray penetration is reduced. High speed imagining results are illustrated in Fig 2.16. where the spray

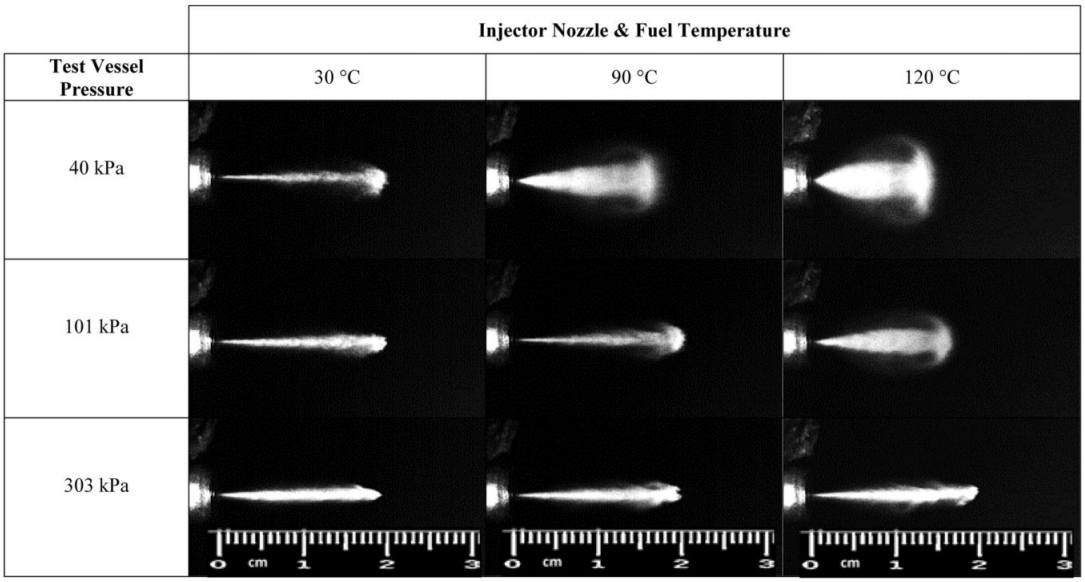

Figure 2.16. Spray Structure after 0.5 ms from ET start (Postrioti et al. (2015))

cone angle gets wider and penetration is reduced when the flash boiling is onset. This images are supported with wider local momentum flux distributions which can be considered fingerprint of the jet (Postrioti et al., 2015). The similar observations were studied by Allocca et al. (2014). Droplet size reduction was observed in some studies (Reitz (1990)). Bianchi et al. (2008) developed a one-dimensional model in which conservation and transport equations for a compressible homogeneous adiabatic two-phase flow were put together with equation of state to link the pressure variation to the density variation via the speed of sound in a suitable thermodynamic relations for the prediction of flash

evaporation in superheated liquid jets. The model was applied to the water injected at 7 bar pressure. The validation were done according to mass flow rate at three different temperatures ranging from 400 K to 499 K and for each temperature at discharge pressure varying between 1 and 5 bar. After validation of this model, Kawano et al. (2004) modelled atomization and vaporization of fuel spray in flash boiling conditions. According to the study, the flash boiling onset occurs in nozzle with bubble nucleation and growth, the fuel was injected with these already existing bubbles and modified TAB breakup model was applied at this stage. The newly formed droplets are also subjected to flash boiling and heterogeneous nucleation and bubble growth computed by Rayleigh-Plesset equation occur and in turn when the bubble volume fraction reaches to a critical value (0.55), this induces the secondary breakup into small droplets twice as many as the number of bubbles.

In this investigation a numerical model is developed to study the effect of flash boiling conditions of GDI injector in a constant volume chamber. To simulate flash boiling effect in terms of wider angle and shorter penetration on spray structure, effervescent atomizer model (Sec. 3.3.2.4) is used with WAVE breakup model.

CHAPTER 3

METHODOLOGY

One of the widely used methods for spray simulations is discrete droplet model (DDM) in which the polydisperse spray formed by atomization is divided into a finite number of droplet classes. A parcel of droplets belonging to each class is tracked along its trajectory until all droplets in the parcel totally evaporated. For track initiation, initial droplet size and velocity distributions are needed.

3.1. Lagrangian-Eulerian Approach for Spray Simulations

A spray penetrates a combustion chamber with a gaseous atmosphere, for which two-phases must be taken into account. Instead of solving the liquid phase as a partial-differential-equation based continuum, the Lagrangian-Eulerian methods which is Discrete Phase Model in FLUENT treats the liquid as discrete particles.

$$F = F(particle, t), \tag{3.1}$$

which is called a Lagrangian representation. If the vector $\overrightarrow{x} = \overrightarrow{x}(particle, t)$ denotes the position, velocity and acceleration are simply given by $\overrightarrow{u} = d\overrightarrow{x}(particle, t)/dt$ and $\overrightarrow{a} = d^2\overrightarrow{x}(particle, t)/dt^2$.

$$F = F(\overrightarrow{x}, t) \tag{3.2}$$

$$\frac{DF}{Dt} = \frac{\partial F}{\partial t} + u_1\frac{\partial F}{\partial x_1} + u_2\frac{\partial F}{\partial x_2} + u_3\frac{\partial F}{\partial x_3}, \tag{3.3}$$

where $\overrightarrow{u} = (u_1, u_2, u_3)$ is the velocity vector. In order to describe a complete flow field,this approach is applied to all points $\overrightarrow{x}$.

3.1.1. Description of Continuous Phase for Evaporating and Non-reacting Sprays

3.1.1.1. Eulerian Representation

If a body is in motion, its physical properties, such as temperature, can change with time. These changes are often described in two different ways: the Lagrangian or the Eulerian formulation. In the Lagrangian formulation, the changes are described with a coordinate system that moves with the body, the material coordinates, whereas in the Eulerian formulation, the physical properties of the body are described with respect to a fixed location in space. It is obvious that the Lagrangian approach is well suited for the description of disperse phases (e.g. sprays consisting of liquid droplets), but not for that of continuous fluids (Baumgarten (2006)).

3.1.1.2. Equations for Gas Phase

Continuity equation:

$$\frac{\partial \rho}{\partial t} + \text{div}(\rho \mathbf{u}) = \dot{\rho}^s, \tag{3.4}$$

where the spray source terms are identified with a superscript, s. The spray source term indicating the mass transfer between the liquid and gas phases due to evaporation is $\dot{\rho^s}$.
Species:

$$\frac{\partial \rho_m}{\partial t} + \text{div}(\rho_m \mathbf{u}) = \text{div}[\rho D \,\text{grad}(\frac{\rho_m}{\rho})] + \dot{\rho}^s \delta_{m,\nu}, \tag{3.5}$$

where the Kronecker delta, $\delta_{m,\nu} = 1$ if m is a fuel species in Eq. 3.5. In Eq. 3.5 the species flux is given by Fick's Law, $\mathbf{J}_m = \text{div}[\rho D \,\text{grad}(\frac{\rho_m}{\rho})]$.

Momentum conservation equation:

$$\begin{aligned} \frac{\partial \rho \mathbf{u}}{\partial t} + \text{div}(\rho\, \mathbf{u}\, \mathbf{u}) &= \text{div}[\sigma - (p + \frac{2}{3}\rho k)\mathbf{I}] + \dot{M}^s + \rho g \\ \sigma &= \mu[(\text{grad}\, \mathbf{u} + (grad\, \mathbf{u})^T) - \frac{2}{3} div \mathbf{u} \mathbf{I}], \end{aligned} \tag{3.6}$$

Energy:

$$\frac{\partial(\rho e)}{\partial t} + \text{div}(\rho e \mathbf{u}) = -\text{div}\mathbf{q} - p\,\text{div}\mathbf{u} + \rho\epsilon + \dot{Q}_s$$
$$q = -K\,\text{grad}T - \rho D \sum_m h_m \text{grad}(\frac{\rho_m}{\rho}), \tag{3.7}$$

In Eq. 3.7 the heat flux vector $\mathbf{u}$ explains the heat conduction by $K\,\text{grad}T$ and the enthalpy diffusion is given by $\rho D \sum_m h_m \text{grad}(\frac{\rho_m}{\rho})$, k and epsilon model turbulence equations:

$$\frac{\partial(\rho k)}{\partial t} + \text{div}(\rho k \mathbf{u}) = \text{div}[(\mu_g + \frac{\mu_t}{Pr_k})\text{grad}\,k] + \sigma : \text{grad}\mathbf{u} - \rho\epsilon - \frac{2}{3}\rho k\,\text{div}\mathbf{u} + \frac{\text{d}W^s}{\text{d}t} \tag{3.8}$$

$$\frac{\partial(\rho \epsilon)}{\partial t} + \text{div}(\rho \epsilon \mathbf{u}) = \text{div}[(\mu_g + \frac{\mu_t}{Pr_k})\text{grad}\,\epsilon] + C_1\frac{\epsilon}{k}\sigma : \text{grad}\mathbf{u} - C_2\rho\frac{\epsilon^2}{k}$$
$$-C_3\rho\epsilon\,\text{div}\mathbf{u} + C_s\frac{\epsilon}{k}\frac{\text{d}W^s}{\text{d}t} \tag{3.9}$$

$\dot{M}_s$ and $\dot{Q}_s$ are spray contributions in the momentum and the energy equations. Beside of these contributions there is also a spray term , $\dot{W}_s$, in both turbulence model equations. Since the turbulence fluctuations perform work on the spray droplets, this term will be negative. The effective viscosity is the sum of the molecular viscosity for the gas phase, μ_g, and the turbulent viscosity μ_t in Eq. 3.13.

$$\mu_t = C_\mu \rho k^2/\epsilon \tag{3.10}$$

$$\mu = \mu_g + C_\mu \rho k^2/\epsilon \tag{3.11}$$

When the value μ is know, the mass diffusivity and heat conductivity are computed from:

$$D = \frac{\mu}{\rho Sc_t} \tag{3.12}$$

$$K = \frac{\mu C_p}{\rho Pr_t} \tag{3.13}$$

where Sc_t and Pr_t are the turbulent Schmidt and Prandtl numbers, C_p is the heat capacity at constant pressure.

3.2. Description of Discrete Phase

3.2.1. Spray Equation

Dispersed spray droplets travel in a gaseous environment. The drop number density differs in the different regions. Further downstream the drop number density is lower than the nozzle region. The probable number of droplets per unit volume at time t and in state $\mathbf{X}$ are represented by probability density approach (Williams (1958)). The state $\mathbf{X}$ of a droplet is described by its parameters which are the location x,the velocity v, the radius r, the temperature T_d, the deformation parameter y and the rate of deformation $\dot{y}$. The formulation of spray PDF is resulted in $f(t, x, v, r, T_d, y, \dot{y})$. While the droplet velocity is represented by $\mathbf{v}$, the gas phase velocity is denoted by $\mathbf{u}$. Time evolution of f can be described in a differential form by a transport equation derived from phenomenological approach;

$$\frac{\partial f}{\partial t} + \mathrm{div}_{\mathbf{x}}(f\mathbf{v}) + \mathrm{div}_{\mathbf{v}}(f\dot{v}) + \frac{\partial(f\dot{r})}{\partial r} + \frac{\partial(f\dot{T_d})}{\partial T_d} + \frac{\partial(f\dot{y})}{\partial y} + \frac{\partial(f\ddot{y})}{\partial \dot{y}} = \dot{f_{coll}} + \dot{f_{bu}}, \quad (3.14)$$

where $\mathrm{div}_{\mathbf{x}}$ and $\mathrm{div}_{\mathbf{v}}$ describes the divergences with respect to the droplets' spatial and velocity coordinates, respectively. $\dot{f_{coll}}$and $\dot{f_{bu}}$ account for the sources due to collision and breakup,respectively. As the rate of change of the quantities such as drop temperature and radius is added into the spray equation (Eq. 3.14), the equation gets more complicated and thus it could not be solved directly. To obtain a convincing solution Stochastic Parcel Technique (Dukowicz, 1980) based on the Monte-Carlo Method. To solve Eq. 3.14 $\dot{v}$,$\dot{r}$,$\dot{T_d}$,$\dot{y}$ and $\ddot{T}_d$ need to be specified.These expressions are explained in the following sections (Sec. 3.2.1.1, Sec. 3.2.1.2)

3.2.1.1. Drop Acceleration

As a droplet moves through a gas, it is distorted significantly when the Weber number is high. Since the droplet drag coefficient highly depends on the droplet shape. Dynamic drag model takes into account for distortions effects.

$$\frac{\mathrm{d}\mathbf{v}}{\mathrm{d}t} = \frac{3}{8} C_D \frac{\rho_g}{\rho_d} \frac{\|\mathbf{v}_r\|}{r} \mathbf{v}_r + g, \quad (3.15)$$

where C_D is drag coefficient; ρ_g, the gas density;ρ_d, the drop density ;$\mathbf{v}_r = \mathbf{u} + \mathbf{u}' - \mathbf{v}$,the relative velocity.The drag coefficient is formulated as in Eq. 3.16.

$$C_D = \begin{cases} \frac{24}{Re_d}(1 + Re_D^{2/3}/6) \text{ if } Re_d \leq 1000 \\ 0.424 \quad \text{if } Re_d > 1000 \end{cases} \tag{3.16}$$

where Re_d is the droplets number which is described as following;

$$Re_d = \frac{2r\rho_g \mathbf{v}_r}{\mu_g(\breve{T})} \tag{3.17}$$

where the viscosity μ_g depends on the weighted gas temperature calculated by:

$$\breve{T} = (T + 2T_d)/3 \tag{3.18}$$

3.2.1.2. Drop Radius

The drop radius change is calculated by the mass rate of change due to evaporation and condensation. When the convective mass transfer is taken into account, the radius rate of change can be described by the Frossling correlation (Froessling (1938));

$$\frac{\mathrm{d}r^2}{\mathrm{d}t} = \frac{\rho_v}{\rho_d} D_v B_d Sh_d, \tag{3.19}$$

Here, D_v is the vapour diffusivity in the gas and is determined by an empirical relation.

$$\rho_v D_v = D_1 \breve{T}^{D_2}, \tag{3.20}$$

where D_1 and D_2 are constants and $\breve{T}$ is calculated from Eq. 3.18.

Spalding mass transfer number B_d is defined as

$$B_d = \frac{Y_v^* - Y_v}{1 - Y_v^*}, \tag{3.21}$$

where $Y_v = \rho_v/\rho_g$ is vapour mass fraction, Y_v^* is the vapour mass fraction on the drop surface calculated from

$$Y_v^*(T_d) = [1 + \frac{W_0}{W_v}(\frac{p_g}{p_v(T_d)} - 1)]^{-1}, \tag{3.22}$$

In Eq. 3.22 W_v is the molecular weight of the vapour and W_0 is molecular weight of the surrounding gas excluding the fuel vapour. While $p_v(T_d)$ is the equilibrium vapour pressure, p_g is the gas phase pressure.
Sherwood number is given by

$$Sh_d = (2.0 + 0.6Re_d^{1/2}Sc_d^{1/3})\ln(\frac{1+B_d}{B_d}), \tag{3.23}$$

The Droplet Schmidt number in Eq. 3.24, Sc_d, is computed by

$$Sc_d = \frac{\mu_g(\breve{T})}{\rho_g D_g(\breve{T})}, \tag{3.24}$$

where $\breve{T}$ is given by Eq. 3.18.

3.2.1.3. Drop Temperature

Spray droplets take heat from surrounding air for evaporation or give heat to surrounding air. When the liquid droplet is applied energy balance, the total heat flux is given by;

$$\dot{Q_{drop}} = \dot{Q_{heating}} + \dot{Q_{evap}}, \tag{3.25}$$

$$\begin{aligned} \dot{Q}_{heating} &= m_d c_{p,l}\frac{\mathrm{d}T_d}{\mathrm{d}t} \\ \dot{Q}_{evap} &= L(T_d)\frac{\mathrm{d}m_d}{\mathrm{d}t} \end{aligned} \tag{3.26}$$

Eq. 3.25 can be expressed by

$$c_d m_d \frac{\mathrm{d}T_d}{\mathrm{d}t} = q_h S_d + L(T_d)\frac{\mathrm{d}m_d}{\mathrm{d}t}, \tag{3.27}$$

Here, C_d is droplet specific heat, q_h is convective heat flux to the drop per unit area and $L(T_d)$ is latent heat of evaporation. The change in the drop temperature heat conduction rate, q_h, is proposed by Ranz and Marshall (1952).

$$q_h = K_g(\breve{T})Nu_d(T - T_d)/2r, \tag{3.28}$$

where the conductivity of the gas, K_g, is calculated by the empirical relation.

$$K_g(\breve{T}) = \frac{K_1\breve{T}^(3/2)}{\breve{T} + K_2} \tag{3.29}$$

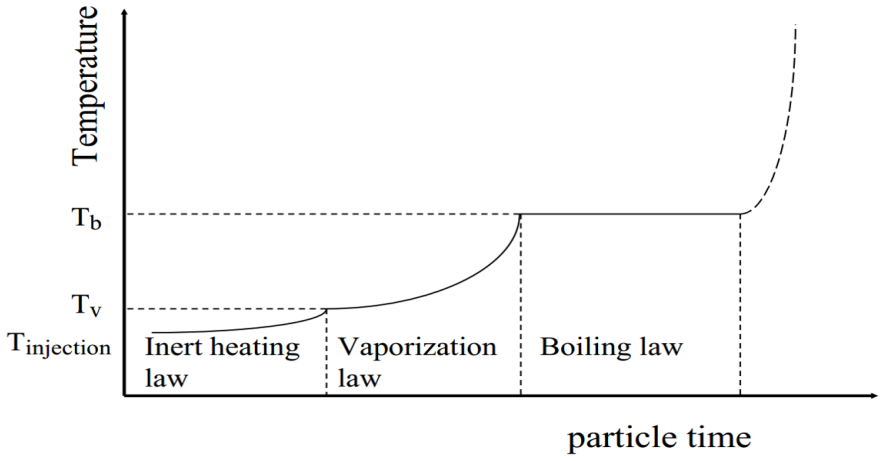

Figure 3.1. Inert heating, vaporization and boiling (Fluent (2009)

where K_1 and K_2 are constants and $\breve{T}$ is given by Eq. 3.18. The Nusselt number which is given below governs the convective heatflux.

$$Nu_d = (2.0 + 0.6Re_d^{1/2}Pr_d^{1/3})\ln\frac{1+B_d}{B_d}, \tag{3.30}$$

Here, Re_d is given by Eq. 3.17 and the Prandtl number is defined by

$$Pr_d = \frac{\mu_g(\breve{T})C_p(\breve{T})}{K_g(\breve{T})}. \tag{3.31}$$

The latent heat of vaporization, $L(T_d)$, is the necessary energy for converting liquid into vapour at the constant vapour pressure.

$$L(T_d) = h_v(T_d) - h_d(T_d, p_v(T_d)) = [e_v(T_d) + \frac{R_0T_d}{W_v}] - [e_d(T_d) + \frac{p_v(T_d)}{\rho_d}] \tag{3.32}$$

where $p_v(T_d)$ is the equilibrium vapour pressure.

3.2.1.4. Drop Distortion

O'Rourke and Amsden (1987) introduced the mathematical model called TAB model which is used for spray aerodynamics breakup using Stochastic Particle Method (Dukowicz (1980)) as well derived from the equations of damped, forced harmonic oscillator. Aerodynamic force represents forcing term, liquid viscosity represents damping force and surface tension denotes restoring force. In Fig. 3.2 x represents the maximum

radial distortion from the spherical surface, deformation parameter is $y = 2x/r$. Drop distortion equation is as following;

$$\ddot{y} + \frac{5\mu_d}{\rho_d r^2}\dot{y} + \frac{8\gamma}{\rho_d r}y = 2\rho_g \left\|\mathbf{v}_r\right\|^2 3\rho_d^2 \tag{3.33}$$

where μ_d is drop viscosity, γ is surface tension and $\mathbf{v}_r$ is the relative drop-gas velocity.

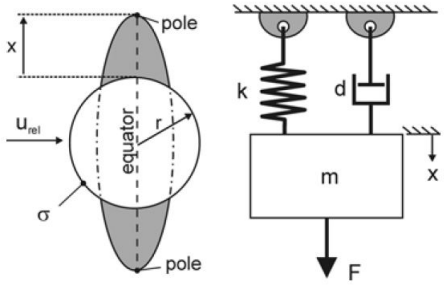

Figure 3.2. Drop Distortion related to a damped, forced oscillator (Baumgarten (2006)

3.2.1.5. Breakup of Drops

Breakup source term, f_{bu}, is in Eq. 3.14. One of the most available model for high Weber number flows is WAVE model which is explained in detail in Sec. 3.3.2.1.

3.2.1.6. Drop Collisions

The source term due to drop collisions ,f_{coll}, are introduced in Eq. 3.14. The most widely used collision model is proposed by O'Rourke (1981). As stated in this model a drop with index 1 most probably goes through n collisions with a drop with index 2 in a given volume V during time interval ΔT. probability to collide can be explained by Poisson distribution;

$$P_n = x^{-n} exp(-\bar{x})/n! \tag{3.34}$$

where $\bar{x} = v\Delta t$ is the mean. The collision frequency with the number of drops in volume V is given by

$$v = \frac{N_2}{V}\pi(r_1 + r_2)^2 \left\|\mathbf{v}_1 - \mathbf{v}_2\right\|, \tag{3.35}$$

There are two possible outcomes on the dependence of impact parameter b which is dependent on collision drop sizes and surface tension when the drops collide. The

drops coalesce if b is less than a critical value $b_c r$. Otherwise, drops go through an elastic collision in which drops exchange momentum but keep their temperature and size.

3.2.2. Coupling Between the Liquid and Gas Phase

While spray droplets are being tracked, they exchange mass,momentum and energy with continuous phase.

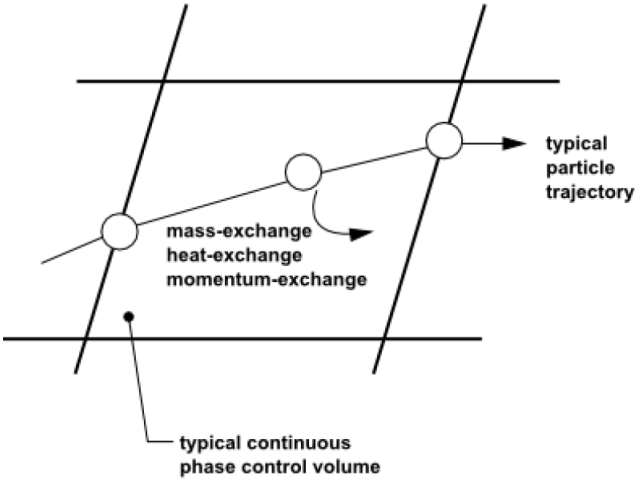

Figure 3.3. Heat, Mass, and Momentum Transfer Between the Discrete and Continuous Phases

3.2.2.1. Spray Source Terms

When all spray submodels are activated, the spray equation $f(t, x, v, r, T_d, y, \dot{y})$ is determined. The sources terms in Eqs. 3.4, 3.5, 3.6,3.7, 3.9 and 3.8 are calculated by summing of the rate of change of mass, momentum and energy of all droplets at a fixed location and time. The mathematical expression of these source terms are given;

$$\dot{\rho_s} = -\int \frac{\mathrm{d}}{\mathrm{d}t}[\frac{4\pi}{3}\rho_d r^3] f d\Omega \tag{3.36}$$

$$\dot{M_s} = -\int \frac{\mathrm{d}}{\mathrm{d}t}[(\frac{4\pi}{3}\rho d r^3 \mathbf{v}) - (\frac{4}{3}\rho_d r^3 \mathbf{g})] f d\Omega \tag{3.37}$$

$$\dot{Q_s} = -\int \left\{ 4\pi\rho_d r^2 \frac{\mathrm{d}r}{\mathrm{d}t}[e_d(T_d) + 0.5(v-u)^2] + \frac{4}{3}\pi\rho_g r^3 [C_d \frac{\mathrm{d}T_d}{\mathrm{d}t} + (\mathbf{F}-\mathbf{g})\mathbf{v}_r] \right\} f d\Omega \tag{3.38}$$

$$\dot{W}_s = -\int \frac{4}{3}\pi\rho_d r^3[(\mathbf{F}-\mathbf{g})u']f\,d\Omega \tag{3.39}$$

where $f\,d\Omega = f(t,\mathbf{X})dv\,dr\,dT_d\,dy\,d\dot{y}$

3.3. NUMERICAL SPRAY MODELING

Discrete Phase Model which is Eulerian-Lagrangian method is provided by Fluent for spray simulations. In the computational domain there are continuous phase co-existing with discrete phase. Fluent offers some submodels for breakup and collision. These models are explained in the following sections in detail.

3.3.1. Break-up Models

3.3.1.1. Primary Breakup

Fluent offers different atomizer types to simulate the spray formation. As in Fig. 2.12, the atomization regime is the related regime for primary break-up. Hence, it is assumed that there is no liquid core; all the liquid is formed into droplets immediately after the exit of the nozzle hole. The atomizer creates initial conditions, that depend on the internal nozzle flow, for further particle trajectory calculations by defining initial droplet diameter, velocity and the cone angle of the spray.

3.3.1.2. Plain Orifice Atomizer Model

In the case of this study the internal nozzle flow state is unknown. The experiments performed are related to spray parameters such as liquid penetration length, momentum flux. Some available phenomenological models can be used for exit velocity, initial droplet
diameter and spray angle or plain orifice model in which these initial parameters are directly calculated according to the state of the internal flow can be employed. Bekdemir et al. (2008) used the Plain Orifice Model in his thesis in the diesel injection conditions.

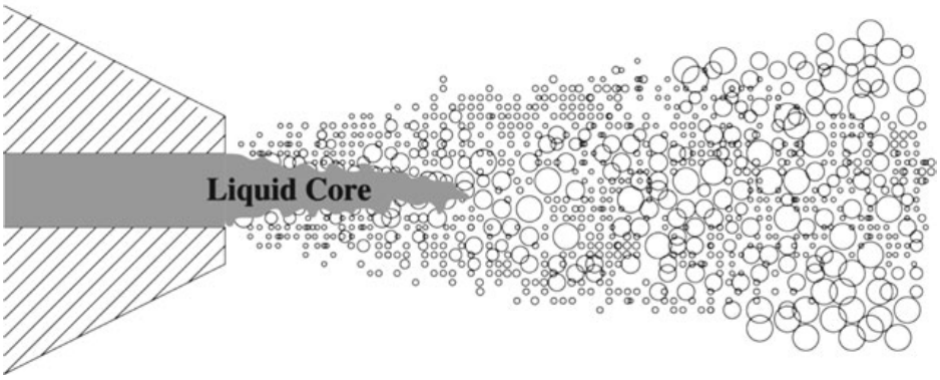

Figure 3.4. External flow structures relevant to plain orifice atomizers (Ashgriz (2011))

Plain orifice model is chosen for primary breakup modelling since the research injector geometry in the study is suitable for this application.

Fluent offers three kinds of nozzle flow, namely single-phase, cavitating and flipped flows (see Fig. 3.5), which was proposed by Soteriou et al. (1995). According to the states, the spray structures change dramatically.

For cavitation number,

$$K = \frac{P_1 - P_{vap}}{P_1 - P_2}, \tag{3.40}$$

Critical value of K,

$$K_{crit} = 1 + \frac{1}{(1 + \frac{L}{4d})(1 + \frac{2000}{Re_h})e^{\frac{70r}{d}}}, \tag{3.41}$$

$$Re_h = \frac{d\rho_l U_{bernoulli}}{\mu}, \tag{3.42}$$

The state of the flow inside the nozzle flow depends on the cavitation number K (see Eq. 3.40), geometrical details such as the radius of the inlet edge of the nozzle r, hole diameter d, and length of the nozzle L (see Fig. 3.5).

$U_{bernoulli}$ is calculated by Eq. 3.45.

Fluent uses the coefficient of contraction C_C proposed by Nurick (1976) (see Eq. 3.43).

$$C_C = \frac{1}{\sqrt{\frac{1}{C_{ct}^2} - \frac{11.4r}{d}}}, \tag{3.43}$$

where C_{ct} originated from potential flow analysis of flipped nozzles equals to 0.611.

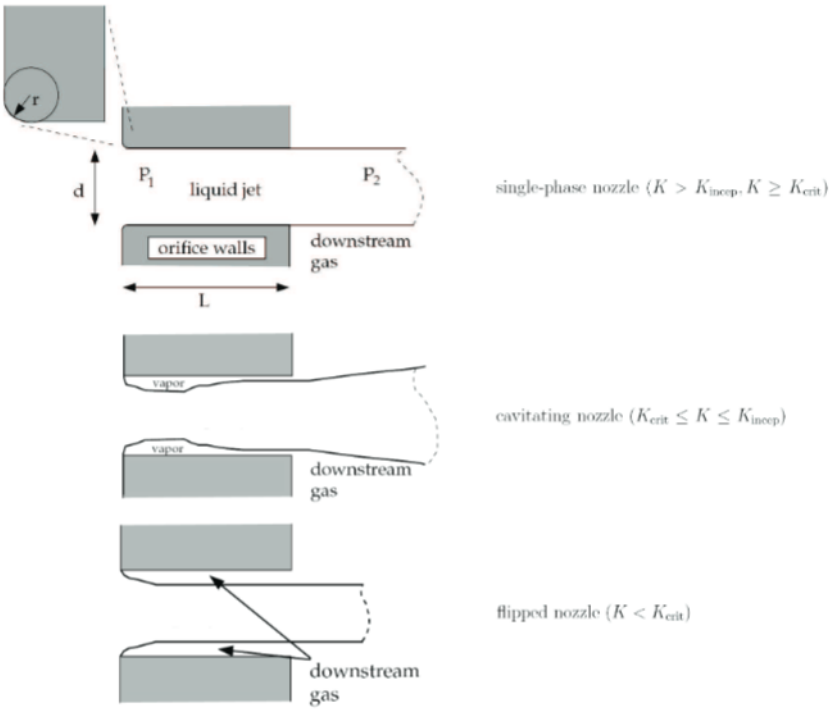

Figure 3.5. Plain orifice atomizer model and decision for flow state (Fluent (2009))

3.3.1.3. Discharge Coefficient

Coefficient of discharge describes the performance of the nozzle. $U_{inj,max}$ is the upper limit for initial velocity calculated from Bernoulli Equation.

$$U_{inj} = \frac{\dot{m}_{inj}}{A_{hole}\rho_l}, \tag{3.44}$$

$$U_{inj,max} = \sqrt{\frac{2\Delta P_{inj}}{\rho_l}}, \tag{3.45}$$

$$C_d = \frac{\dot{m_{eff}}}{\dot{m_{bernoulli}}} = \frac{\rho_l A_{hole} u_{mean}}{\rho_l A_{hole} u_{bernoulli}} = \frac{u_{mean}}{\sqrt{2(P_0 - P_2)\rho_l}}, \tag{3.46}$$

After the decision of the state of the internal flow,the discharge coefficients are calculated as follows: For a cavitating flow (Nurick (1976));

$$C_d = C_c\sqrt{K}, \tag{3.47}$$

For a flipped flow (Nurick (1976));

$$C_d = C_{ct} = 0.611, \tag{3.48}$$

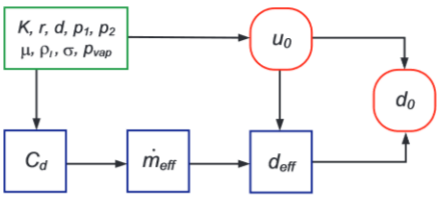

Figure 3.6. Atomizer Scheme (Bekdemir et al. (2008))

3.3.1.4. Exit Velocity

To initiate tracking of spray droplets initial velocity must be specified. Initial velocities are given in the following expressions.

For single phase,

$$u = \frac{\dot{m_{eff}}}{\rho_l A}, \tag{3.49}$$

For flipped flow,

$$u = \frac{\dot{m_{eff}}}{\rho_l C_{ct} A}, \tag{3.50}$$

For cavitating flow proposed by (Schmidt and Corradini (1997)),

$$u = \frac{2C_c P_1 - P_2 + (1 - 2C_c)P_v}{C_c\sqrt{2\rho_l(P_1 - P_v)}}, \tag{3.51}$$

3.3.1.5. Spray Angle

To define the initial direction, the spray angle should be defined. The correlation of Ranz (1958) used in the model in Eq. 4.2.

$$tan(\frac{\theta}{2}) = \frac{2\pi}{3C_A}\sqrt{\frac{3\rho_g}{\rho_f}}, \tag{3.52}$$

According to the correlation of Reitz and Bracco (1982) C_A is calculated via Eq. 3.53.

$$C_A = 3 + \frac{L}{3.6d}, \tag{3.53}$$

For flipped flow;

$$\theta/2 = 0.01 \tag{3.54}$$

3.3.1.6. Droplet Diameter Distribution

According to the scheme in Fig. 3.6, after calculating the exit velocity and inputing the measured $\dot{m}_{eff}$ initial droplet diameters need to be computed depending on the flow states. Sauter Mean diameter d_{32} represents the average droplet diameters (see Eq. 2.5).

For single phase the correlation of Wu et al. (1992) is used,

$$d_{32} = 133\frac{d}{8}We^{-0.74} \tag{3.55}$$

For cavitating flow the same correlation but d replaced by d_{eff} given by Eq. 3.57 due to the contraction in the cross sectional area of the nozzle,

$$d_{32} = 133\frac{d_{eff}}{8}We^{-0.74}, \tag{3.56}$$

$$d_{eff} = \sqrt{\frac{4\dot{m}_{eff}}{\pi\rho_l u}}, \tag{3.57}$$

For flipped flow the most probable diameter,

$$d_0 = d\sqrt{C_{ct}}, \tag{3.58}$$

The Sauter Diameter Sizes are related to the most probable diameter for Rosin Rammler distribution.

$$d_0 = 1.2726 d_{32}\left(1 - \frac{1}{s}\right)^{1/s} \tag{3.59}$$

where s is spread parameter given by Table 3.1.

Table 3.1. Spread Parameters

State	**Spread parameter**
Cavitating flow	3.5
Single phase flow	1.5
Flipped flow	∞

3.3.2. Secondary Breakup Models

Already existing drops are subjected to secondary breakup into smaller droplets. Simulation for secondary breakup WAVE model (Reitz and Diwakar, 1987) is widely used (Postrioti and Battistoni (2010), Bekdemir et al. (2008)).

3.3.2.1. WAVE Model

Reitz and Diwakar (1987) developed a numerical model for diesel sprays, their results showed good agreement with experimental data in the core region containing large drops near the nozzle and predicting the length of core region, which agreed with measurements in dense spray. However their model was not accurate showing the fuel vapour region. An improved model was proposed by Reitz (1987), allowing a new atomization model so-called WAVE that added new parcels containing product drops to the computation and agreed with the experimental data.

The Wave model is suitable for high-speed injections ($We > 100$) (Fluent (2009)). This model considers the breakup of the droplets to be induced by the relative velocity between the gas and liquid phases. The formation of child droplets from parent droplets is induced by the growth rate of Kelvin-Helmholtz instabilities on the liquid surface.

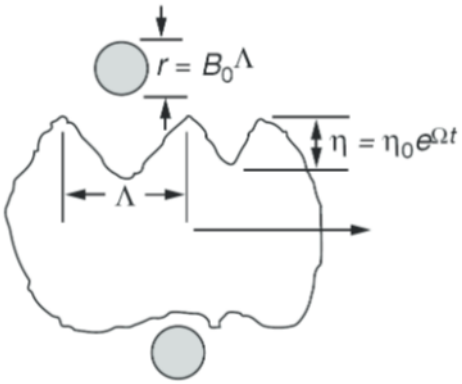

Figure 3.7. Sketch of the Wave Model

$$\frac{\Lambda}{a} = 9.02\frac{(1+0.45Oh^{0.5})(1+0.4Ta^{0.7})}{(1+0.87We_2^{1.67})^{0.6}}, \tag{3.60}$$

$$\Omega\sqrt{\frac{\rho_l a^3}{\sigma}} = \frac{(0.34+0.38We_2^{1.5})}{(1+Oh)(1+1.4Ta^{0.6})}, \tag{3.61}$$

where subscript 1 is for the liquid phase,subscript 2 is for gas.As shown by Reitz and Bracco (1982) in Eqs. 3.60 and 3.61, Ω is maximum growth rate and Λ is the corresponding wavelength.$Oh = \sqrt{We_1}/Re_1$ is the Ohnesorge number and $Ta = Oh\sqrt{We_2}$ is the Taylor number.

According to the model radius of newly formed droplets are proportional to the

wavelength of the fastest-growing unstable surface wave.

$$r = B_0\Lambda, \tag{3.62}$$

The rate of change of droplet radius in the parent parcel is given by

$$\frac{da}{dt} = -\frac{(a-r)}{\tau}, r \leqslant a, \tag{3.63}$$

where the breakup time τ is in the Eq.3.64

$$\tau = \frac{3.726B_1a}{\Lambda\Omega}, \tag{3.64}$$

Λ and Ω are calculated by Eqs. 3.60 and 3.61. The constant $B_0 = 0.61$ in the work of Reitz and Bracco (1982). The breakup time constant can vary between 1 and 60, which depends on the injector characterization. However, in the work of Liu et al. (1993) it is recommended that B_1 is set to 1.73.

When the shed mass reach 5% of the the initial mass, a new parcel is created which have the same properties excepting radius and velocity. The radius of new parcel is given by the Eq. 3.62. The new parcel is given a component of velocity randomly selected in the plane orthogonal to the direction vector of the parent parcel, and the momentum of the parent parcel is adjusted so that momentum is conserved. The velocity magnitude of the new parcel is the same as the parent parcel.

3.3.2.2. Kelvin-Helmhotz Rayleigh-Taylor (KH-RT Model)

This model combines the Kelvin-Helmholtz waves induced by aerodynamic forces with the Rayleigh-Taylor instabilities due to acceleration of shed drops ejected into freestream conditions. This model is only for high We number sprays. It is assumed that there is a liquid core near the nozzle and child droplets are shed from this core (see Fig. 3.8). The liquid core length is figured out by Levich Theory(Levich et al. (1962)).

$$L = C_L d_0 \sqrt{\frac{\rho_l}{\rho_g}}, \tag{3.65}$$

where C_L is Levich constant and d_0 is a reference nozzle diameter. The blobs are introduced into the domain (see Fig. 3.8). The diameter specified in the injection. It is often best to use an effective droplet diameter by considering a contraction coefficient, which can be computed with

$$D_e = \sqrt{C_a} d_0, \tag{3.66}$$

where C_a term represent contraction coefficient.

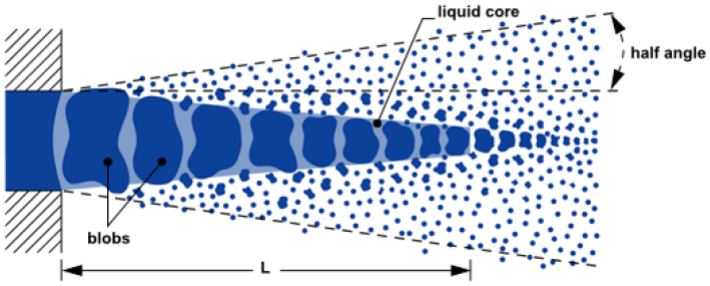

Figure 3.8. KH-RT Approach (Fluent (2009))

3.3.2.3. Rayleigh-Taylor Breakup

While droplet and gas are moving with relative velocity u_{rel} to each other, the deceleration of the droplet induced by drag force can be treated as an acceleration in the direction of airflow. This can cause instabilities on the back side of the drop (see Fig. 3.9). As with the Wave model R-T model is based on the wave instabilities on the

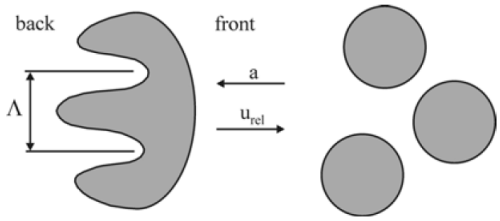

Figure 3.9. Rayleigh-Taylor instability on a liquid droplet (Baumgarten (2006))

droplet surface. The growth rate of the fastest-growing wave Ω and the corresponding wave number K_{RT} are given by

$$\Omega_{RT} = \sqrt{\frac{2}{3\sqrt{3\sigma}} \frac{[a(\rho_l - \rho_g)]^{3/2}}{\rho_l + \rho_g}} \tag{3.67}$$

$$K_{RT} = \sqrt{\frac{-a(\rho_l - \rho_g)}{3\sigma}} \tag{3.68}$$

If R-T waves have been growing for a time larger than the breakup time τ_{RT}, breakup occurs. If the predicted wavelength corresponding to the fastest wave growth rate is smaller than the local droplet diameter. The radius of child droplets is given by Eq. 3.70.

$$\tau_{RT} = \frac{C_\tau}{\Omega_{RT}}, \tag{3.69}$$

$$r_c = \frac{2\pi C_{RT}}{K_{RT}}, \tag{3.70}$$

where C_{tau} is the Rayleigh-Taylor breakup constant which is set equal to 0.5 and C_{RT} is the breakup radius constant whose default value is 0.1. In the liquid core only Wave Model in which only aerodynamics effect is considered is governed. Outside the liquid core both KH and RT effects are considered. A new parcel is generated if the shed parcel mass exceeds 5% of the initial parcel mass.

3.3.2.4. Effervescent Atomizer Model for Flash Boiling Atomization

In effervescent atomizers a gas that may or may not be miscible with the liquid is introduced before atomization takes place (see Fig 3.10). Fluent computes the initial velocity and initial effective diameter as it does for flipped flow (see Eq. 3.71, see Eq. 3.50 respectively). Drop size is sampled from Rosin Rammler distribution (Eq. 3.72). It is needed to specify the spray-half angle and dispersion constant beside of the mass flow rate and the nozzle diameter (see Eq. 3.75).

$$d_{max} = d\sqrt{C_{ct}} \tag{3.71}$$

$$d_0 = d_{max} e^{(-\frac{\theta}{\Theta_s})^2} \tag{3.72}$$

$$\Theta_s = \frac{x}{C_{eff}} \tag{3.73}$$

Mixture quality is defined by;

$$x = \frac{\dot{m}_{vapor}}{\dot{m}_{vapor} + \dot{m}_{liquid}} \tag{3.74}$$

$$\Theta_s = \frac{x}{C_{eff}}, \tag{3.75}$$

where Θ_s is dispersion angle multiplier, C_{eff} is dispersion constant.

3.4. Numerical Setup

Firstly, the domain was designed and was discretized into a grid. Then, boundary conditions and numerical parameter were set. Numerical parameters were set in Table 3.2 and Fig. 3.11 illustrates the boundary conditions.

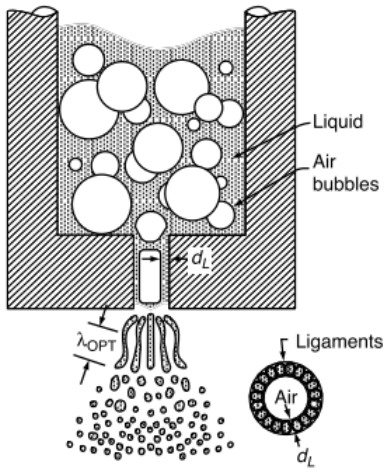

Figure 3.10. Effervescent Atomizer (Moyne (2010))

To mention about numerical settings in literature, whereas Bekdemir et al. (2008) used the timestep of 1e-6 with a grid size of 0.1 mm, which is approximately equal to the minimum grid size in the studies of Postrioti et al. (2011), Postrioti and Battistoni (2010), Kösters and Karlsson (2011) used 0.5x0.5x1 mm grid size and same time-step value. However Postrioti et al. (2011) and Postrioti and Battistoni (2010) had the timestep of 5e-6 and Postrioti et al. (2009) used the time-step of 2e-6. Hence, in this study the time-step of 1e-6 and grid size are highly suitable.

Table 3.2. Numerical settings

Turbulence model	standard k-epsilon
Injected Parcels	300
Initial k	3e-7
Initial epsilon	1e-9
Initial velocity	0.01 m/s
Grid size	max 0.2 min 0.1
Time-step	1e-6
Fuel	n-heptane
Scheme	SIMPLE

Breakup Models and Drag Model

The primary and secondary break-up and drag model used are listed:

- Plain Orifice Atomizer Model for Initial droplets (see Sec.3.3.1.2)(Bekdemir et al. (2008))

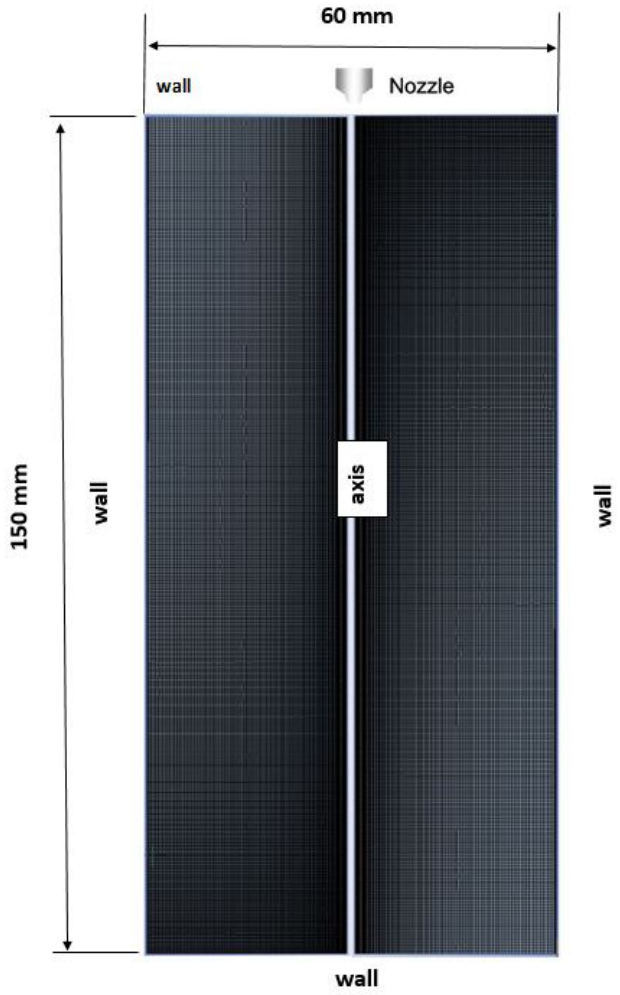

Figure 3.11. Boundary Conditions

- WAVE Breakup Model (see Sec.3.3.2.1) Main tuning constants were $C_1 = 0.61$ and $C_2 = 30$ for WAVE model.
- Spherical Drag Model (see Sect. 3.2.1.1)

As injection mass flow rate, the measured mass flow rate at 100 bar is fluctuating as in Fig. 3.12.

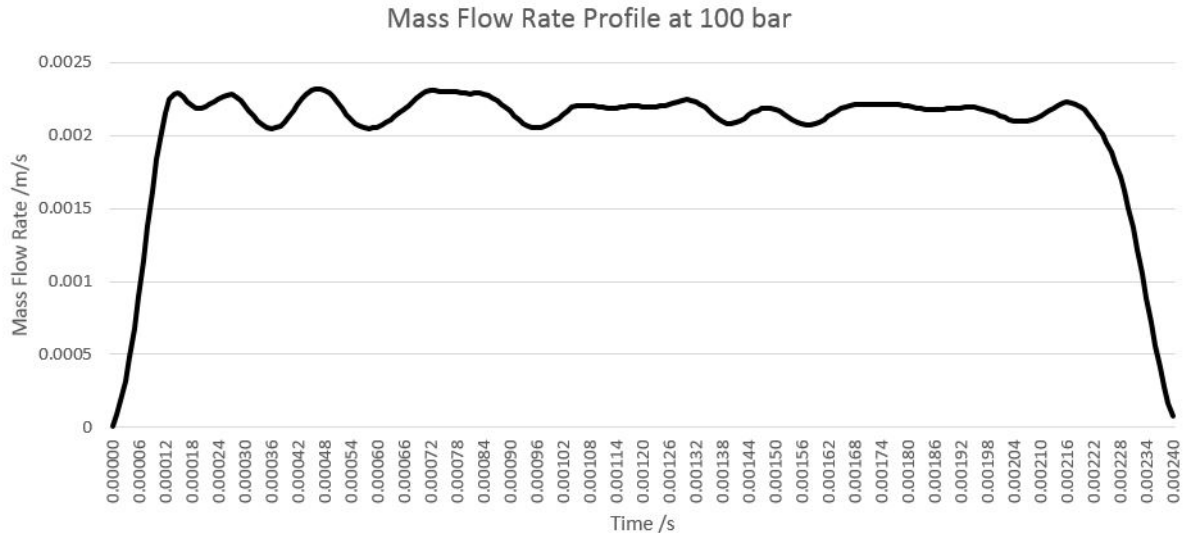

Figure 3.12. Injection Mass Flow Rate Time dependent profile

Table 3.3. Cases at 100 bar injection pressure

	Pinj 100 bar	
Case	**T(K)**	**Pv(kpa)**
1	293	100
2	363	
3	393	
4	293	303
5	363	
6	393	
7	293	40
8	363	
9	393	

Table 3.4. Ambient to Saturation Pressure

Ambient to Saturation Pressure(ATSPR)			
Tfuel(C)	Pa(Kpa)		
	40	100	300
20	8.47	21.38	64.16
90	0.51	1.28	3.85
120	0.22	0.55	1.65

3.5. Mesh and Time-step Dependency

The grid resolution is quite fine and time-step is small enough. Hence, there is no need to check mesh and time-step dependency.Because in study of Kösters and Karlsson (2011) the simulation was run with a grid size of 0.4 mm and with timestep of 1e-6.

3.6. Grid Dependency

The adequate resolution is a necessity for accurate spray simulations as in all numerical simulations. The finer grid becomes, the more accurate solution of Navier-Stokes equations is carried out. However, grid resolution is limited by the computational resources and time. So some researchers tried to reduce the effect the grid resolution. In this chapter it is discussed what an adequate resolution should be and some approaches are included from the point of minimization of spray grid dependencies.

According to the study of Abraham (1997), jet cross-sectional area must have at least four grid cells. Otherwise, the spray is not simulated in a adequate accuracy since the spray is effected by selection of the ambient turbulent and length scales. Meanwhile, the idea of reducing grid size enough to provide mesh-dependency for gas phase near the nozzle disagrees with the void fraction criteria that must be near one. In other words, the volume fraction which the Lagrangian liquid phase must occupy in the cell must be lower than 0.1. For this reason, in the region near the nozzle the gas flow can not be solved accurately.

Grid size influence on the relative velocity is depicted in Fig. 3.14 and the dotted lines represents the staggered grid. The cell containing node 4, which is transferred the momentum source by the drop due to its nearest location, have the same velocity with the node 4. Hence, the finer the grid, the better spatial solution for the gas velocity and thus more accurate droplet-gas momentum exchange. This approach is valid for all transfers

as mass, energy which is added to the nearest node to the liquid parcel. The lower the grid size, the faster momentum source diffuses over the complete cell, and thus influences a smaller area. In the case of higher grid resolution the droplets injected at early times transfers their momentum to small gas volumes and thus causes faster change of gas velocity. Consequently, lower relative velocity slows the rate of increase of the velocity of droplets due to drag force on the proportionally dependence of relative velocity (see Fig. 3.14), which results in lower spray penetration. The number of nodes which is transferred the momentum inversely proportional effects the acceleration of gas velocity (see Fig. 3.13). To keep the coupling of the phases away from mesh dependency, some approaches was improved instead of nearest approach. Schmidt and Senecal (2002) developed a new approach in which a weighted average of gas velocities from neighbouring nodes was taken to provide grid size dependency of the gas velocity (see Fig. 3.15). Before taking weighted average the velocities from neighbouring nodes was transformed in polar coordinates aligned with the injection, subsequently the average was calculated and the result was tranformed in cartesian coordinates again. The reason of the transformation was the fact that while spray was reproduced with resolution at ninety degree angles on cartesian coordinates, polar components of velocity were constant around the atomizer. Namely, the spray was naturally polar.

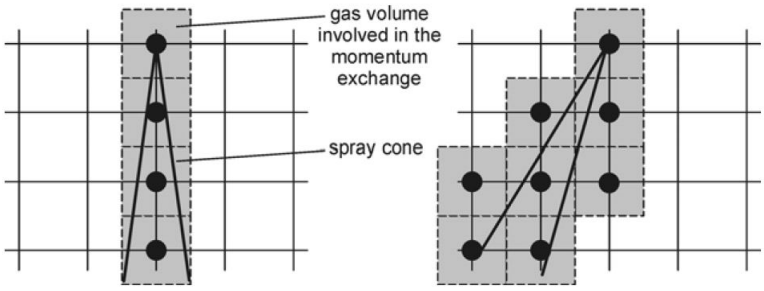

Figure 3.13. Dependency on grid resolution and orientation (Baumgarten, 2006)

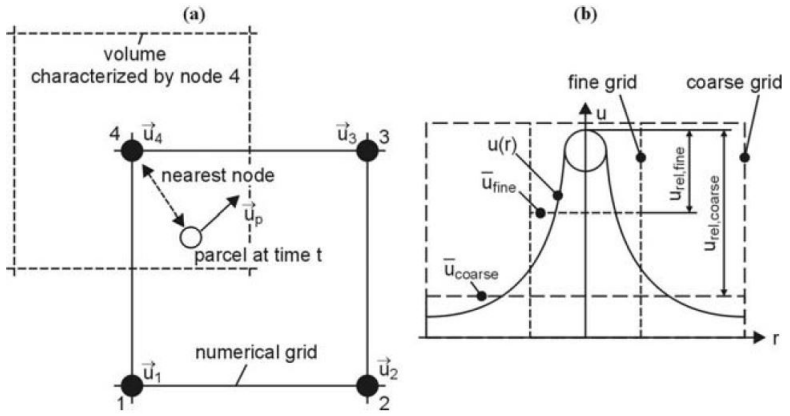

Figure 3.14. The effect of refining the grid on relative velocity during momentum exchange (Baumgarten, 2006)

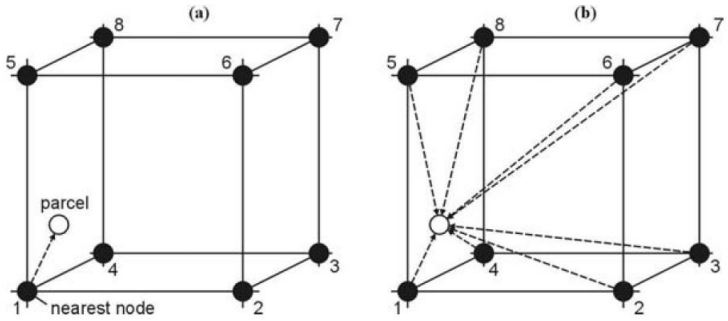

Figure 3.15. A weighted average instead of nearest node approach (Baumgarten, 2006)

Since the penetration of vaporizing spray is very sensitive to the grid size, Gonzalez D et al. (1992) improved a new model in which the vapour is kept in a sphere with the radius proportional to $\sqrt{D_v t}$ until the sphere volume reaches the volume of cell (see Fig. 3.16). This approach is extended correspondingly to momentum coupling in the Couplage Lagrangian-Eulerian (CLE) method proposed by Beard et al. (2000).

In addition to the most widely used and grid dependent collision model of O'Rourke (1981) (for detail see Sec. 3.2.1.6), a new collision algorithm called NTC (No-Time-Counter) which had been used for intermolecular collisions was implemented for spray droplets collision modelling by Schmidt and Rutland (2000). This new method, in which a separate collision mesh is used, relieves the spray collision simulations of mesh dependency and computational costs. To overcome the problems of grid dependency and poor statistical convergence in the dense spray some alternative models such as Interactive Cross-sectionally Averaged Spray (ICAS) Method (Wan and Peters, 1997) in which

the liquid core length and spray cone angle is assumed to be constant have been developed to avoid mesh dependency and bad statistical convergence in the dense region. As a result of the assumptions in this method the 1d spray sources along spray axis are obtained (see Fig. 3.17). In this method cross-sectionally averaged quantities of mass, momentum and energy for both the gas and the liquid phases are given by Eqs. 3.76 and 3.77.

$$\frac{\partial(\hat{\rho}(1-\hat{y}_l)b^2)}{\partial t} + \frac{\partial(\hat{\rho}\hat{u}_g(1-\hat{y}_l)b^2)}{\partial x} = \rho_g \beta b \hat{u}_g + \hat{\omega_{vap}} b^2 \tag{3.76}$$

$$\frac{\partial(\hat{\rho}\hat{y}_l b^2)}{\partial t} + \frac{\partial(\hat{\rho}\hat{u}_g\hat{y}_l)b^2)}{\partial x} = -\hat{\omega_{vap}} b^2 \tag{3.77}$$

where r is the spray radius, $\hat{y}_l$ is liquid fuel mass fraction, $\hat{\rho}_g$ is the mixture density and $\hat{u}_g$, $\hat{u}_l$ are the gas an liquid velocity, respectively. β is the global quantity for turbulent exchange between these two phases.

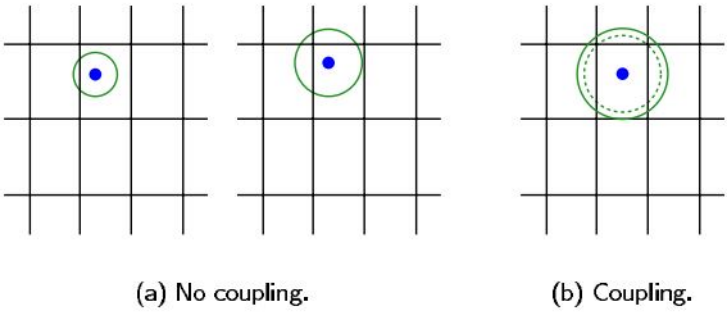

Figure 3.16. Geometrical criterion for vapor mass coupling (Beard et al., 2000)

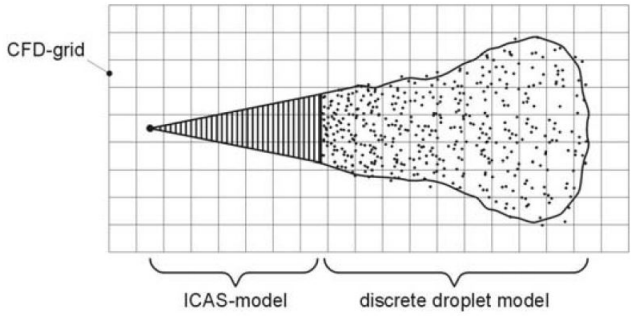

Figure 3.17. Interactive Cross-sectionally Averaged Spray (Stiesch, 2013)

In the book of Stiesch (2013) some suggestions are mentioned for reduction of grid

dependency. Firstly, turbulence length scale needs to be limited to the jet diameter since the jet dominates the mixture formation and flow. The length scale limitation to the nozzle diameter was applied by the authors (Kösters and Karlsson (2011)) with the correlation for k and epsilon. Secondly, the standard k-ϵ model must be modified according to the study of Pope (1978).

3.7. Model Validation

The validation was done according to the penetration and spray angle results for IHP-279 injector whose length to diameter ratio equals to 3. While Fig. 3.18 shows the comparison between the experimental and numerical results for the case 1 (see Table 3.3), Fig. 3.19 does for the case 3 (see Table 3.3).

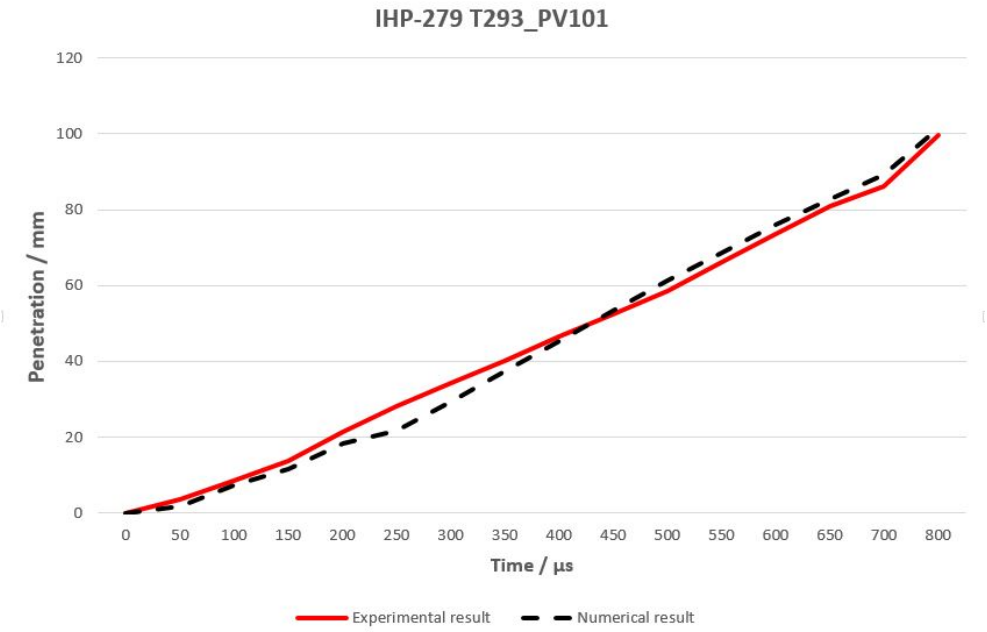

Figure 3.18. IHP-279 Penetration results comparison for Case 1

The validation gives sufficiently satisfactory results in spray penetration results. The model is implemented IHP-293 GDI injector whose length to diameter ratio is 3 for nine cases reported in Table 3.3.

Figure 3.19. IHP-279 Penetration results comparison for Case 3

CHAPTER 4

RESULTS AND DISCUSSIONS

In this study the main aim is to develop a numerical model for predicting the spray structure in terms of spray angle and penetration under flash-boiling and non-flash boiling. The operating conditions are combinations of three fuel temperature (293 K, 363 K, 393 K) and chamber pressure (40 kPa, 101 kPa, 303 kPa). The comparisons for each operating cases are depicted in Figs. 4.3- 4.11.

4.1. Experimental Tests

Experimental tests are done in a constant volume chamber. The constant volume chamber has four windows which can withstand with operating pressure ranges and allows to observe and install fixtures inside it. The chamber pressure and fuel temperature are adjusted depending on operating cases. The time-resolved spray images shown in Fig. 2.16 are taken by means of high speed imaging , which in turn the images are converted into binary format. The boundary of spray is determined through image analysis by image processing codes (see Fig. 4.1). Spray angle depicted in Fig. 4.2 is calculated by taking into account of 60% of the liquid length. Threshold to take into account grey and white pixels are put for these calculations.

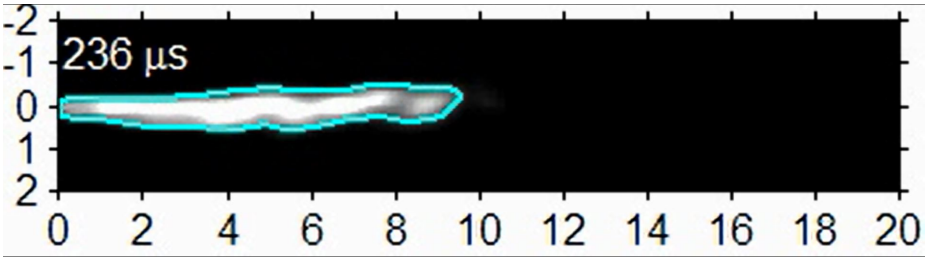

Figure 4.1. Spray Boundary (Pickett et al., 2011)

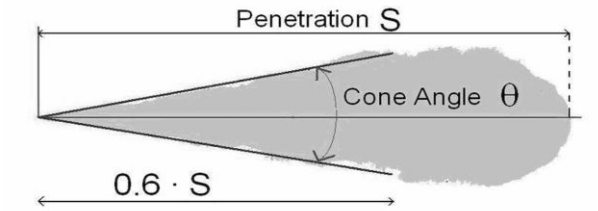

Figure 4.2. Spray Angle Measurement (Desantes et al., 2006)

4.2. Liquid Penetration and Spray Angle Results

For the liquid penetration, the definition by Pickett et al. (2014), as the farthest axial position for 0.1% liquid volume fraction was employed. Fig. 4.3 shows the comparison of spray penetration and spray angle for the case at ambient pressure (Pv) 101 kPa and fuel temperature (Tf) 293 K. It can be seen that the penetration increases slowly during the first 100 μs that how much time takes the needle to lift to the fully opened from its seat. As shown in Fig. 3.12 the injection rate profile can be divided into three phases; needle opening, transition and needle closing. The numerical results have a good agreement with the experiments. However, the spray angle is overpredicted until 650 μs. After this time it seems to agree with experimental results.

Fig. 4.4 shows the results for the case at the same ambient pressure with higher fuel temperature 363 K. It is expected slightly more evaporation resulting in a little shorter penetration when compared to the case for fuel temperature 293 K. The eye-catching jump in spray penetration results incurs the overprediction between 50 and 200 μs. After this time in terms of spray penetration and 500 μs in terms of spray angle the numerical results approximately agree. Prior to 500 μs there is an increase followed by a gradual drop in spray angle between 250 and 450 μs.

Fig. 4.5 depicts the comparison for the case of fuel temperature 393 K at the concerning pressure which is the transition to flash boiling from non-flash boiling. Under these conditions, the evaporation rate is believed to significantly increase and spray angle gets wider due to flash boiling effect. As it is understood from experimental results that spray penetration is shorter than those belonging to the cases of fuel temperature 363 and 393 K. Whereas spray penetration is well predicted, the spray angle does not match the experimental data although its trends seem similar. The slope of first decrease seems close numerical spray angle drops previously to almost 30° and it must show a gradual

decrease. In contrast to this, it remains constant.

Fig. 4.6 illustrates the results for fuel temperature 293 K and at 40 kPa chamber pressure. Spray penetration grows slowly in needle opening period followed by a gradual increase. However spray angle are not predicted well excepting the period after 600 μs.

Fig. 4.7 represents the case for the same pressure and 363 K fuel temperature, which is the transition. In this case more fuel evaporated is expected than in the previous one, which results in shorter penetration. During first 250 μs the results in terms of spray penetration have a good agreement with experimental data. However after this time spray penetration is overpredicted. In terms of spray angle the trend is similar of the case for fuel temperature 393 K and chamber pressure 101 kPa, which is the transition case. In contrast to the same trend with experimental data, the model overpredicts spray angle.

Fig. 4.8 describes the comparisons belonging to the only fully flash boiling case at the concerning pressure and Tf=393 K. Flash boiling is believed to cause the spray wider and shorter penetration due to sudden evaporation. Comparing to other transition cases spray penetration is poorly predicted during periods after the first 250 μs. Spray angle follows the same trend as in the other transition cases for fuel temperature 363 K at the same pressure and 393 K at ambient pressure 101 kPa. That is because the effervescent atomizer model is used for all these cases.

Fig. 4.9 exposes the comparison at ambient pressure 303 kPa which fuel experience late injection shortly after or during compression stroke and fuel temperature 293, spray penetration results follows the experimental data during needle opening phase (first 100 μs). After this phase the line graph of spray penetration graphics increase considerably followed by a gradual increase. In terms of spray angle is dropped sharply in needle opening followed by a sudden increase until almost 150 μs. After this time, spray angle remains constant followed by a steady drop with overprediction.

Fig. 4.10 depicts the results for fuel temperature 363 K at the same pressure conditions in which fuel has more tendency to evaporation than in the previous one. Spray penetration is quite predicted until 200 μs followed by underprediction. The increase in spray penetration is at the same slope followed by a sharp increase the period between 750 and 800 μs. Although initial spray angle match experimental data, while the rest of period spray penetration is poorly predicted. After the decrease in spray angle until 200 μs, the spray angle should drop at a steady rate. However the line graph of spray angle shows fluctuating trend.

Fig. 4.11 illustrates the comparison for fuel temperature 393 K at the concerning pressure. In terms of spray penetration it is expected that the evaporation causes to

decrease the rate of increase in spray angle after a while. In contrast to this, spray penetration rate of change does not decrease and result in overprediction after almost 550 μs. Until this time spray peentration is fairly predicted. During the first 250 μs the overprediction is caused by misestimation of initial spray angle. The slope of line graphs are almost the same during the first 250 μs when compared with experimental data. After this time the graphs shows a sharp increase followed by a sudden drop and fluctuating trend with overprediction.

In general point of view, the ability of prediction of the model depends on the operating conditions. The model works in some operating conditions and during some periods. In contrast to his ability, the model does not predict the spray angle and spray penetration well. The reason is believed to be caused by the plain orifice atomizer model. That is because the initial nozzle state changes over time according to plain orifice atomizer model. Discussion over the results depending on cases is discussed in detail in Chapter 5.

The average deviations between experimental and numerical results are reported in Table 4.1. It can be understood that generally spray angle results highly deviate for all operating cases, which reaches maximum value for 363 K fuel temperature at 3 bar and 0.4 bar ambient pressure.

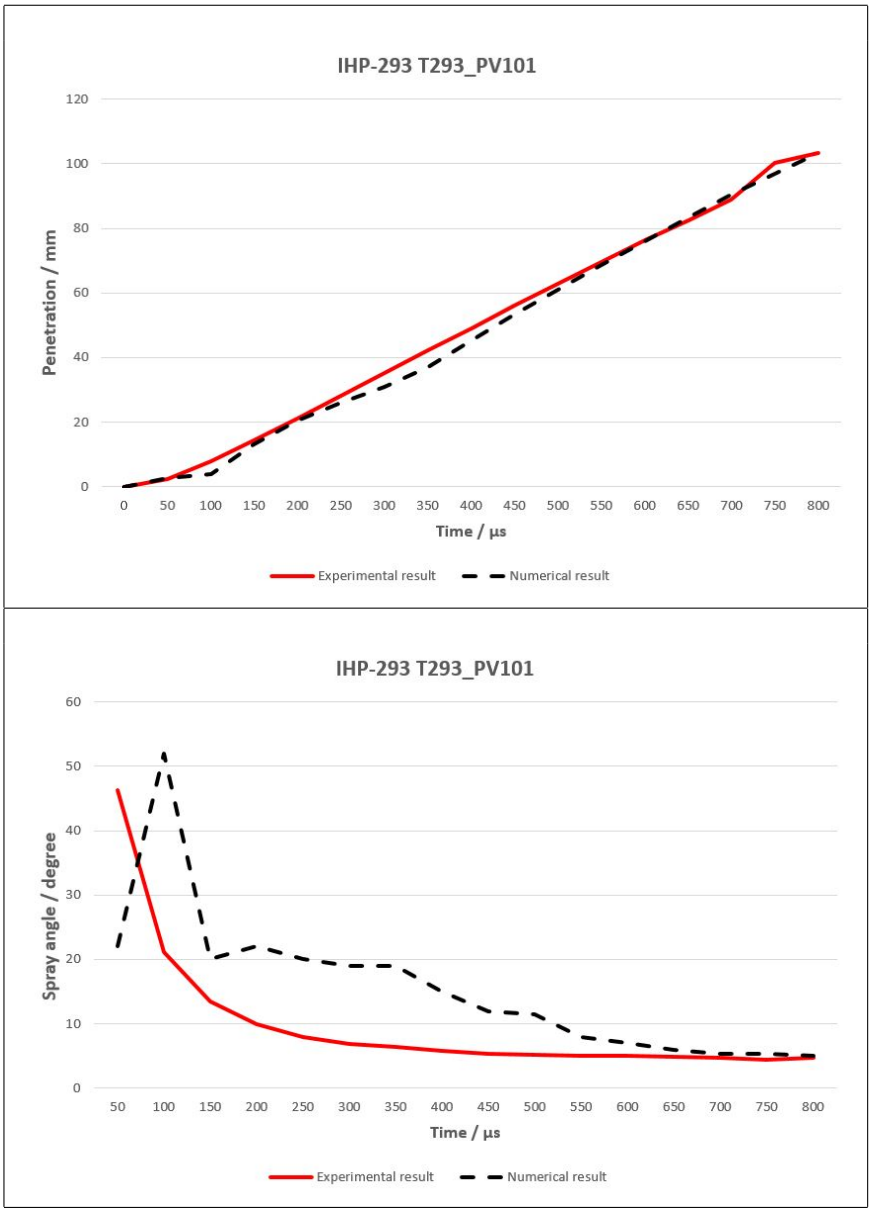

Figure 4.3. Penetration and Spray angle results for Tf=293 K Pv=101 kPa

Table 4.1. Average Deviations for all data points

Chamber Pressure(kPa)	Fuel Temperature (K)	Spray Penetration	Spray angle
40	293	14.68%	54.75%
101		8.43%	91.25%
303		31.91%	61.23%
40	363	17.60%	117.65%
101		55.97%	43.37%
303		25.18%	105.30%
40	393	28.10%	43.36%
101		8.08%	80.86%
303		18.06%	94.34%

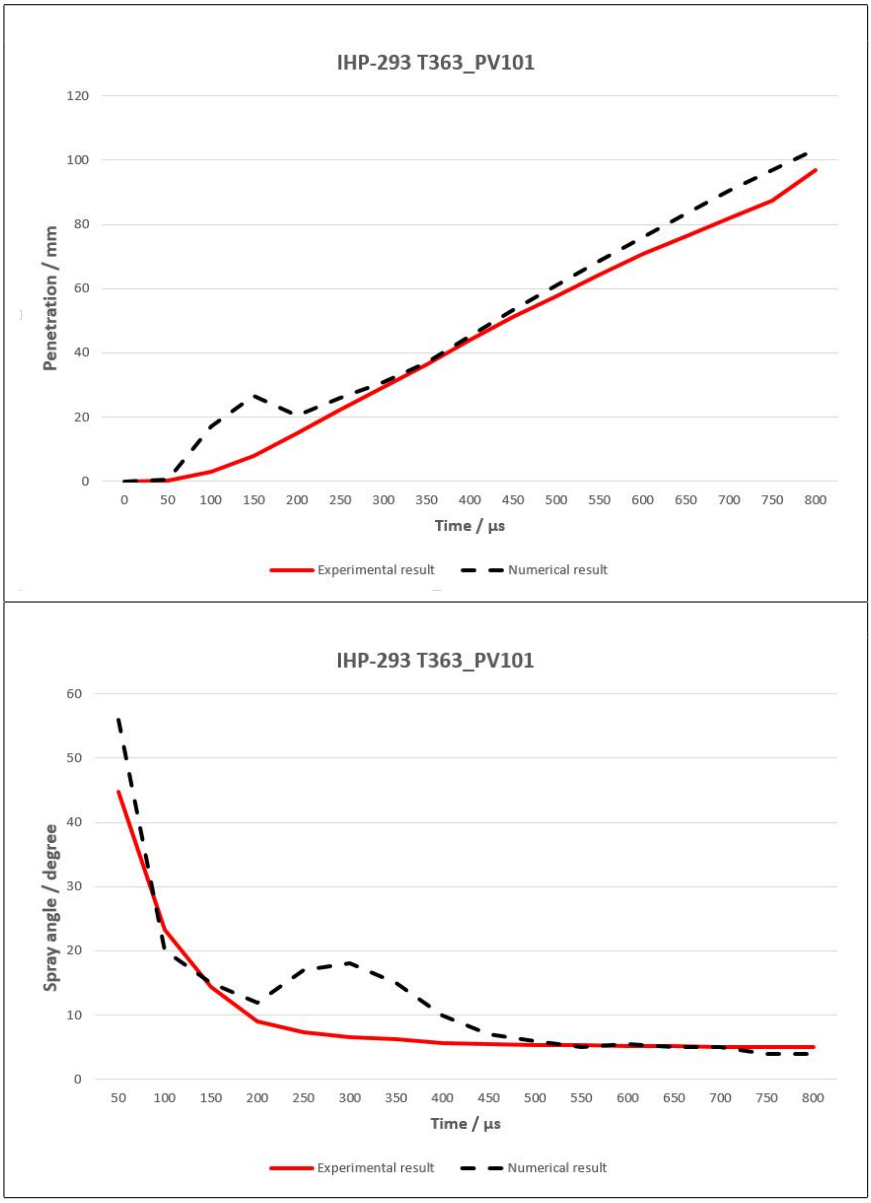

Figure 4.4. Penetration and Spray angle results for Tf=363 K Pv=101 kPa

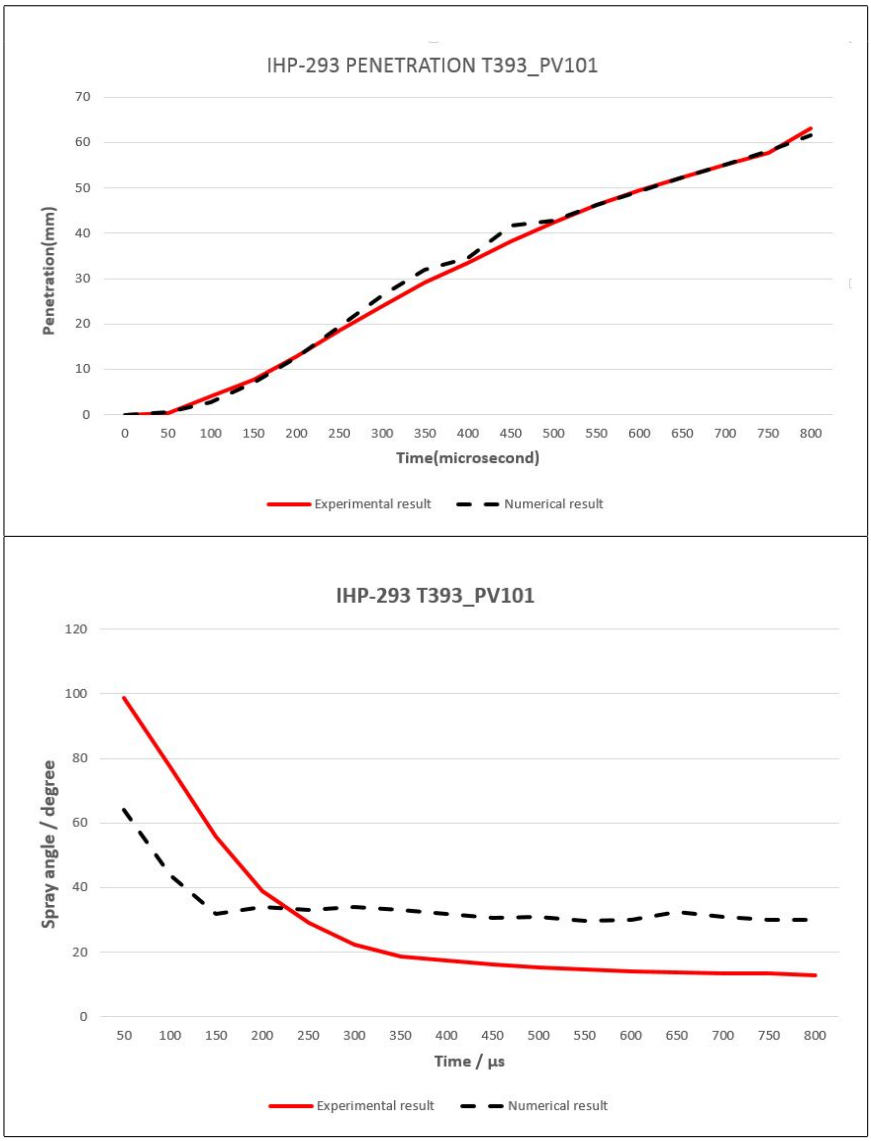

Figure 4.5. Penetration and Spray angle results for Tf=393 K Pv=101 kPa

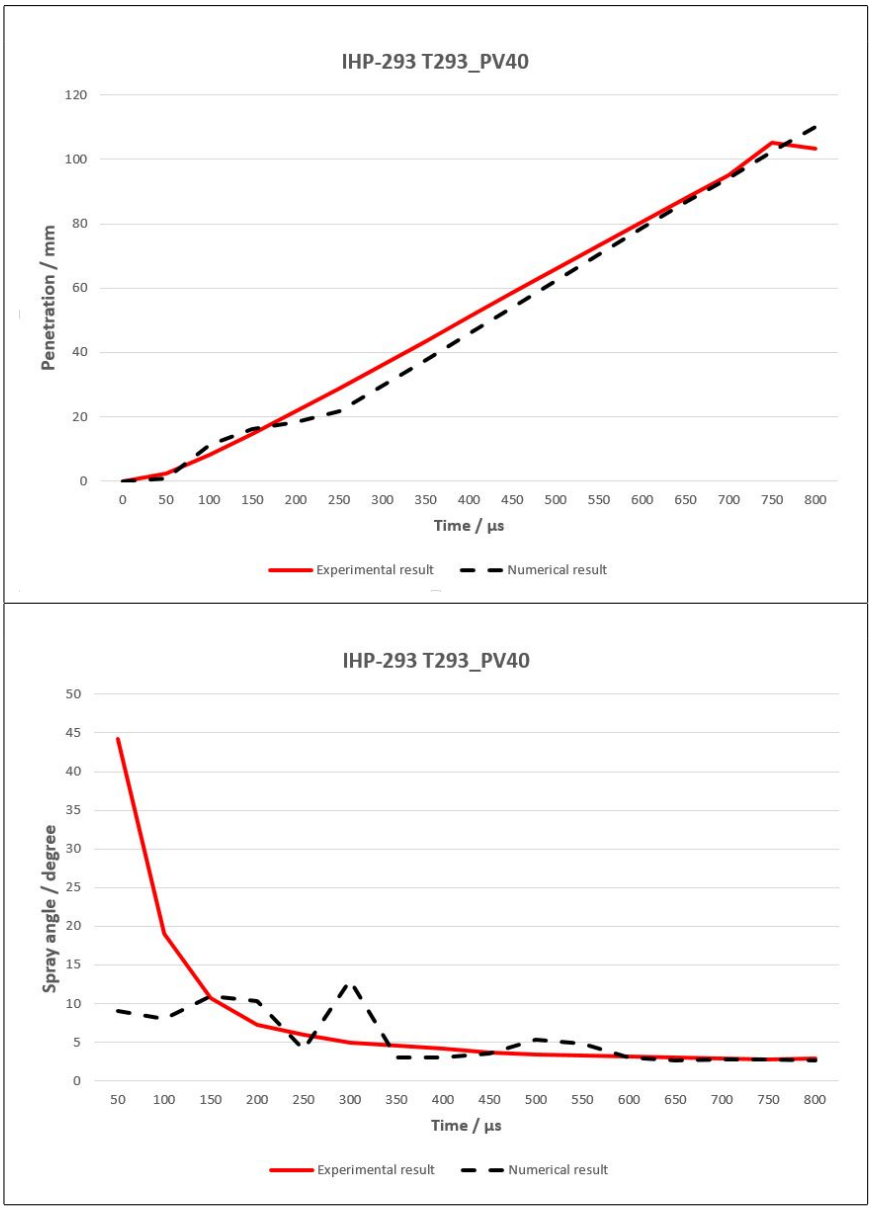

Figure 4.6. Penetration and Spray angle results for Tf=293 K Pv=40 kPa

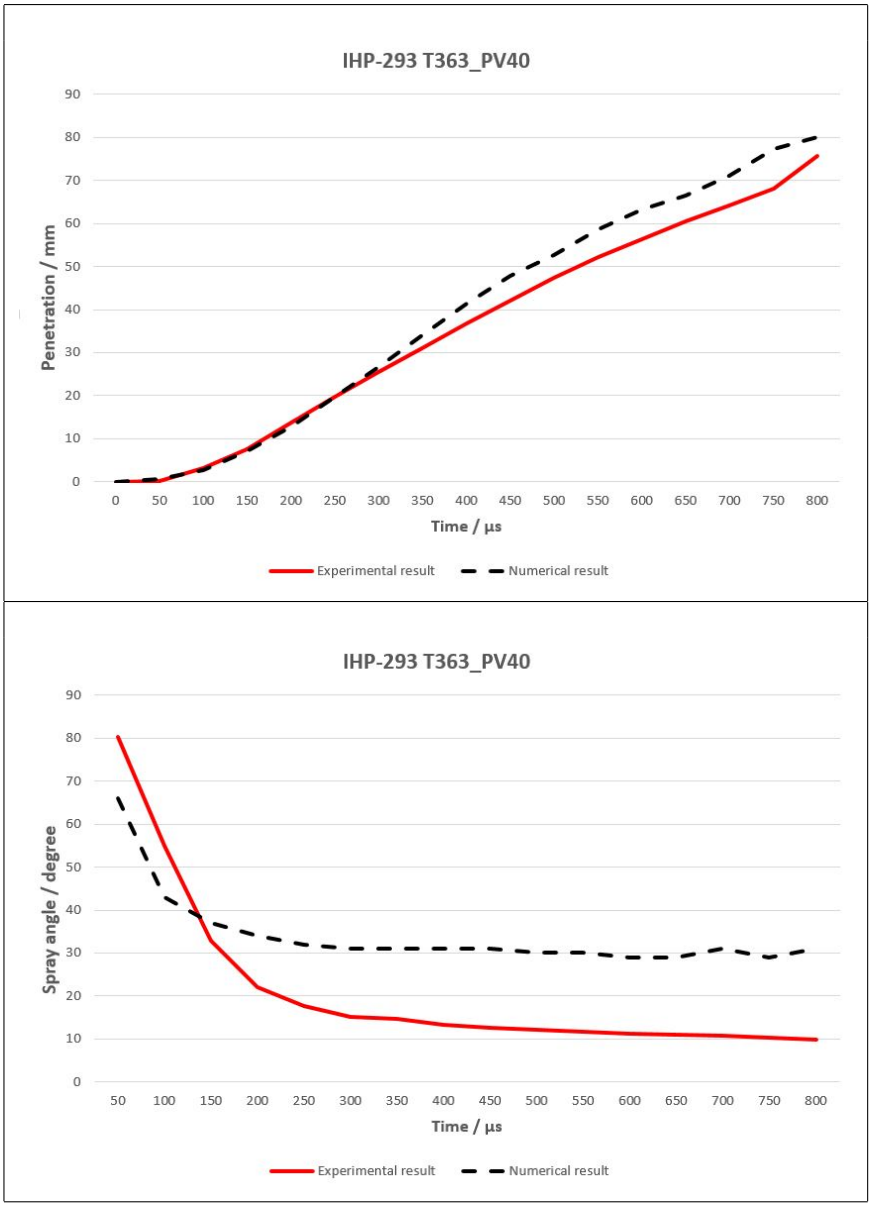

Figure 4.7. Penetration and Spray angle results for Tf=363 K Pv=40 kPa

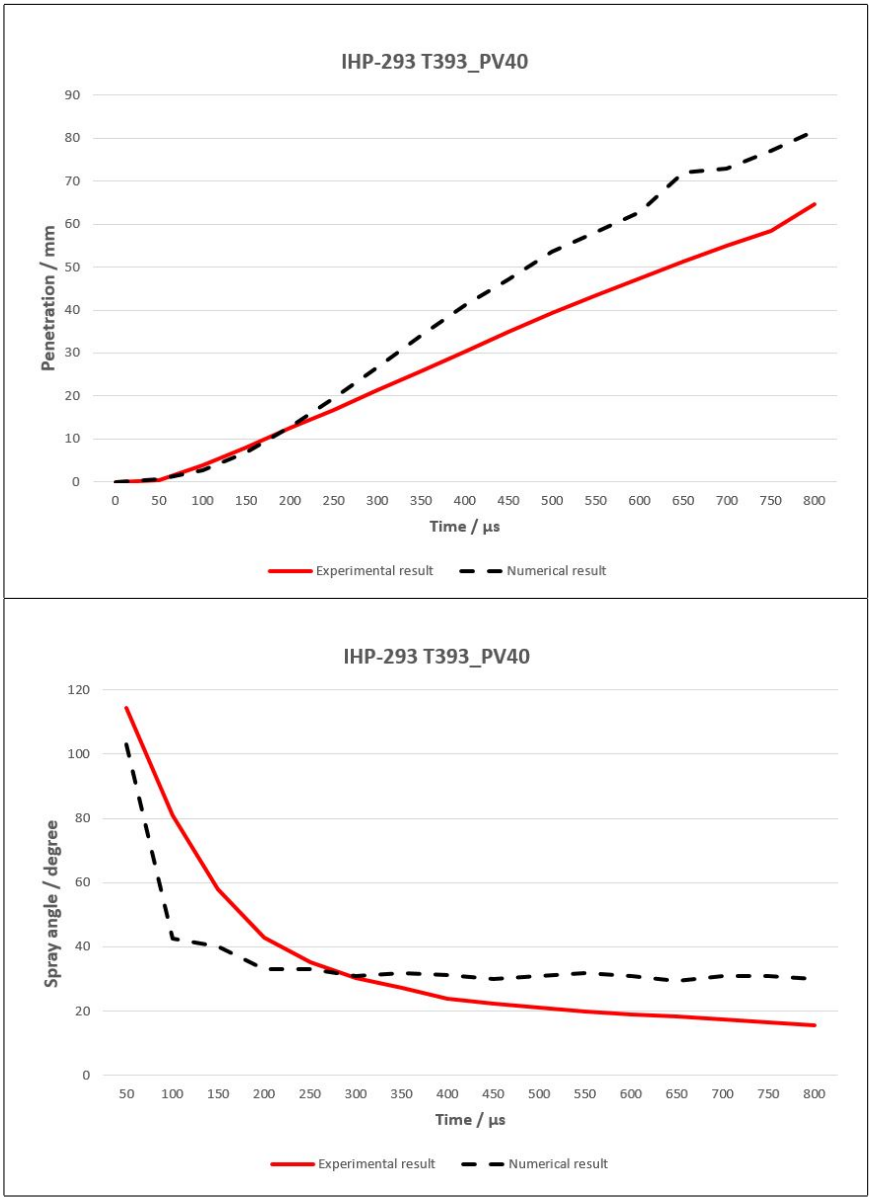

Figure 4.8. Penetration and Spray angle results for Tf=393 K Pv=40 kPa

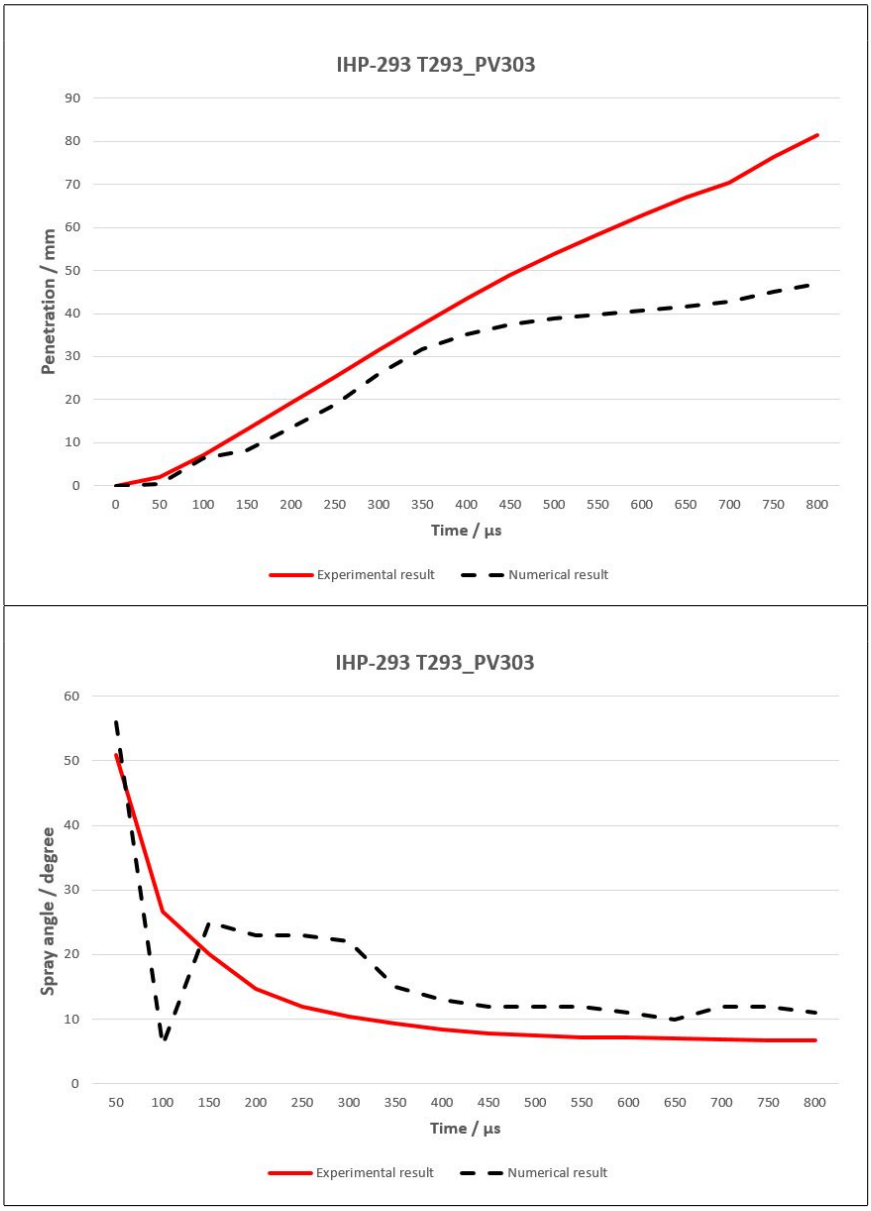

Figure 4.9. Penetration and Spray angle results for Tf=293 K Pv=303 kPa

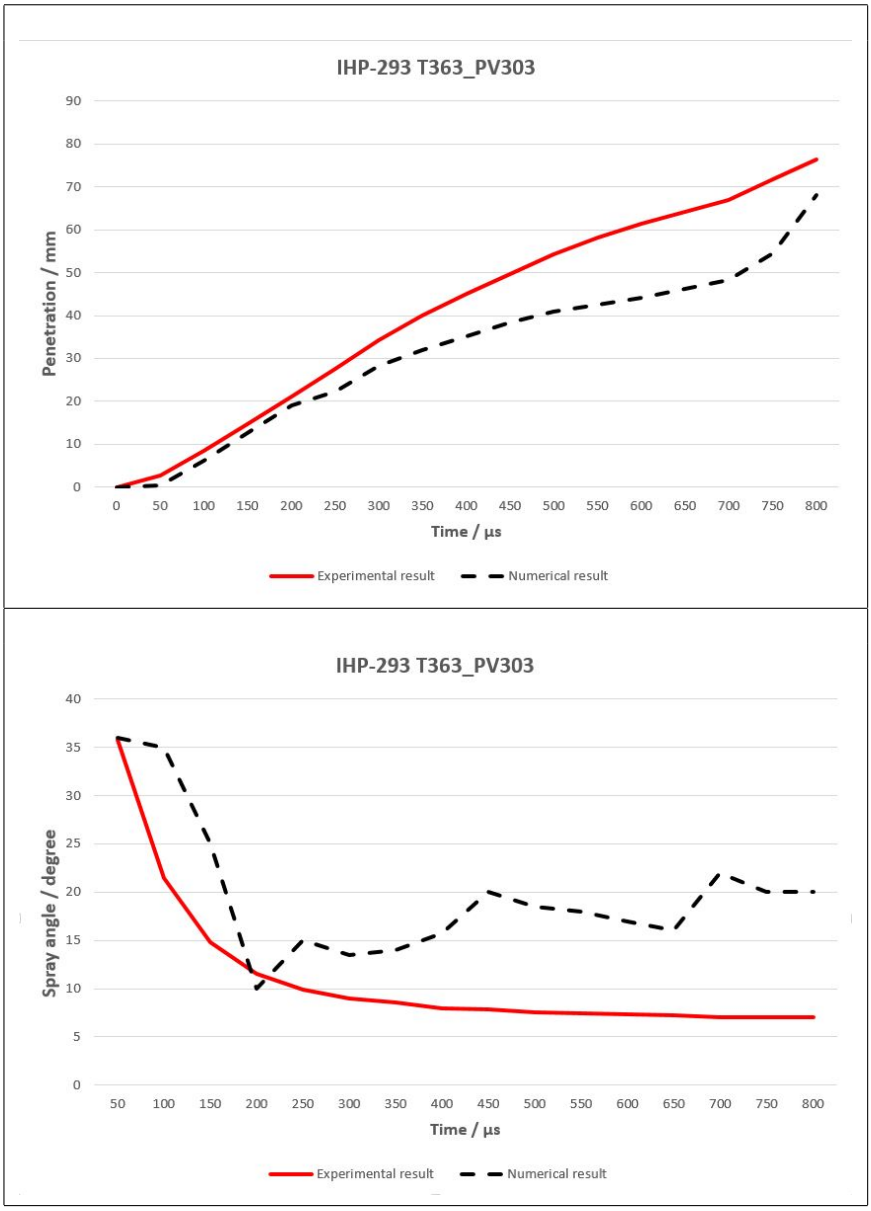

Figure 4.10. Penetration and Spray angle results for Tf=363 K Pv=303 kPa

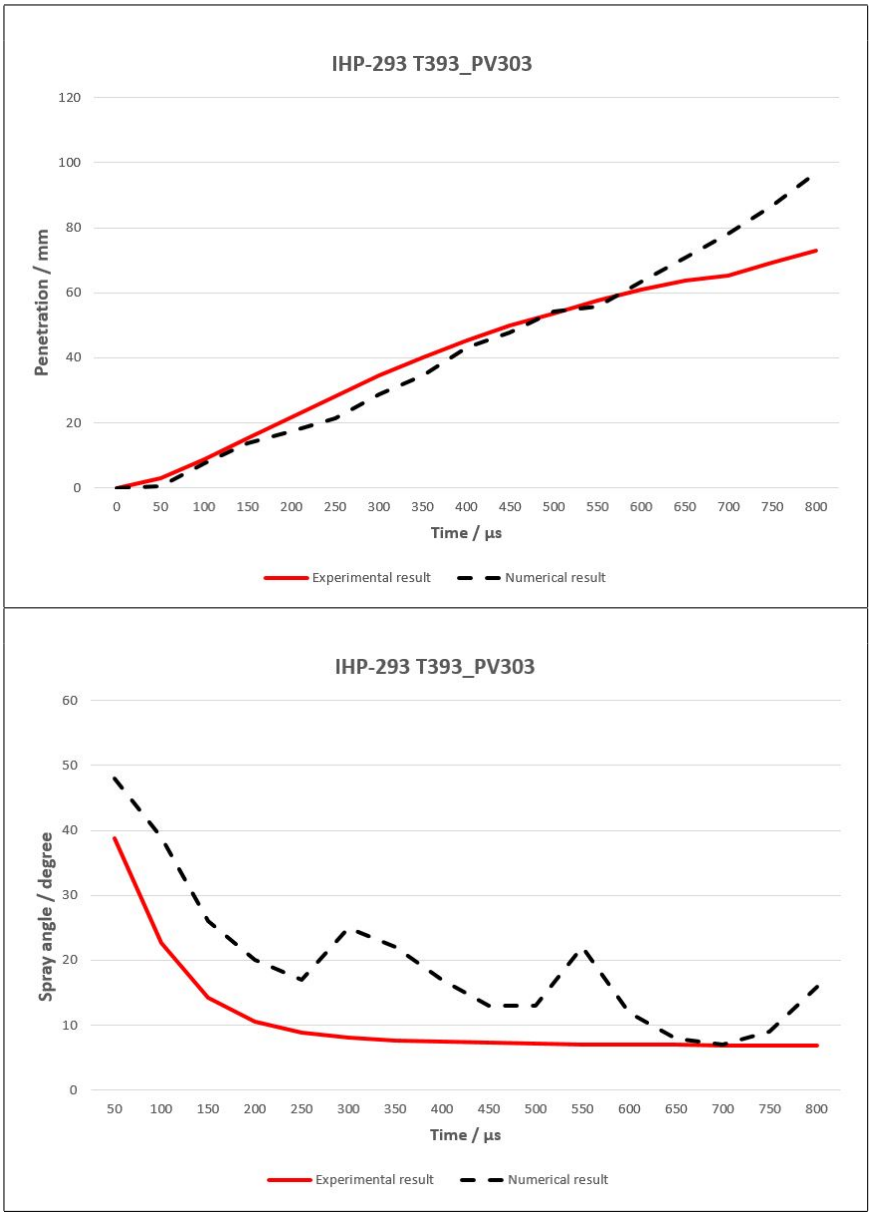

Figure 4.11. Penetration and Spray angle results for Tf=363 K Pv=303 kPa

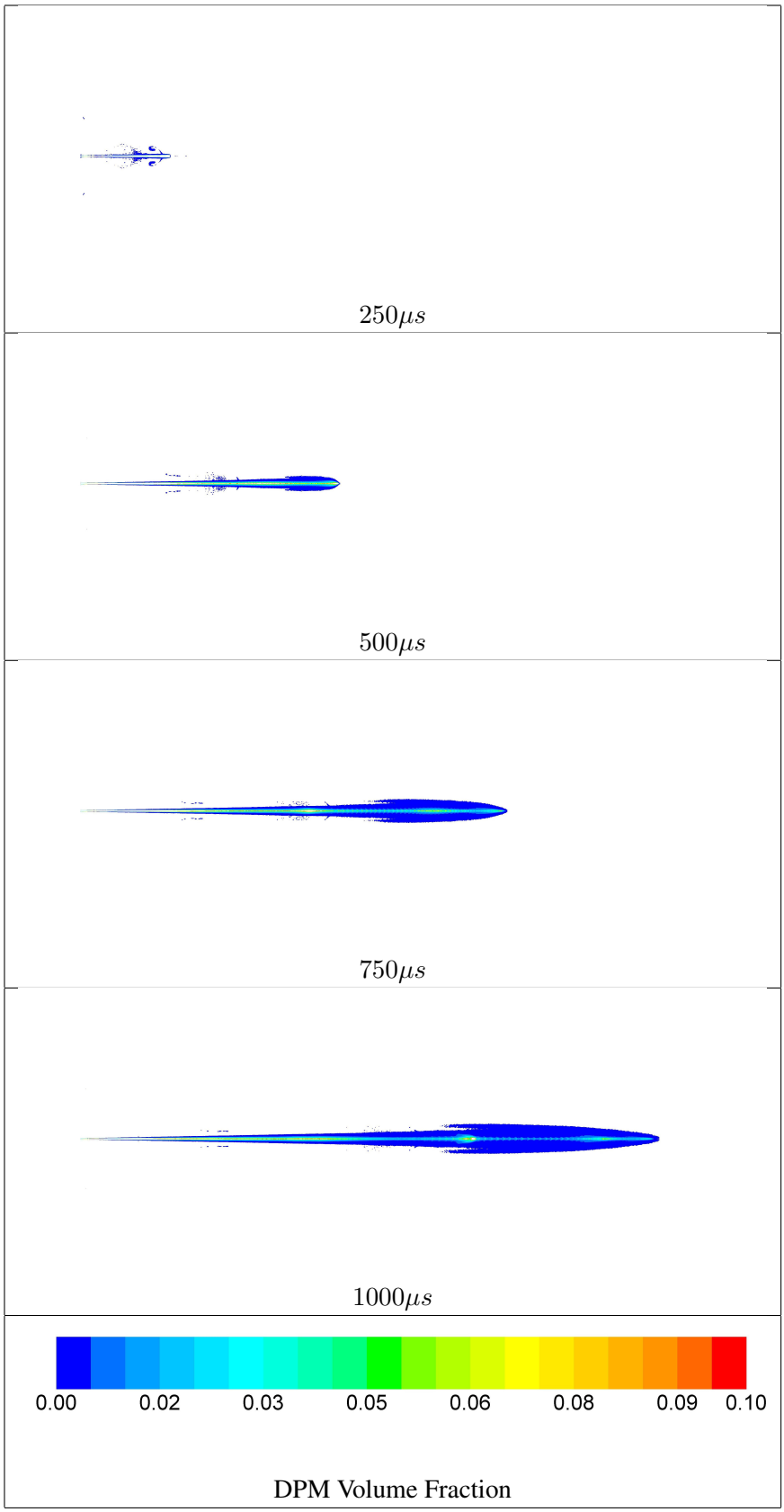

Figure 4.12. Liquid Volume Fraction for T=20 Pv=40 kPa

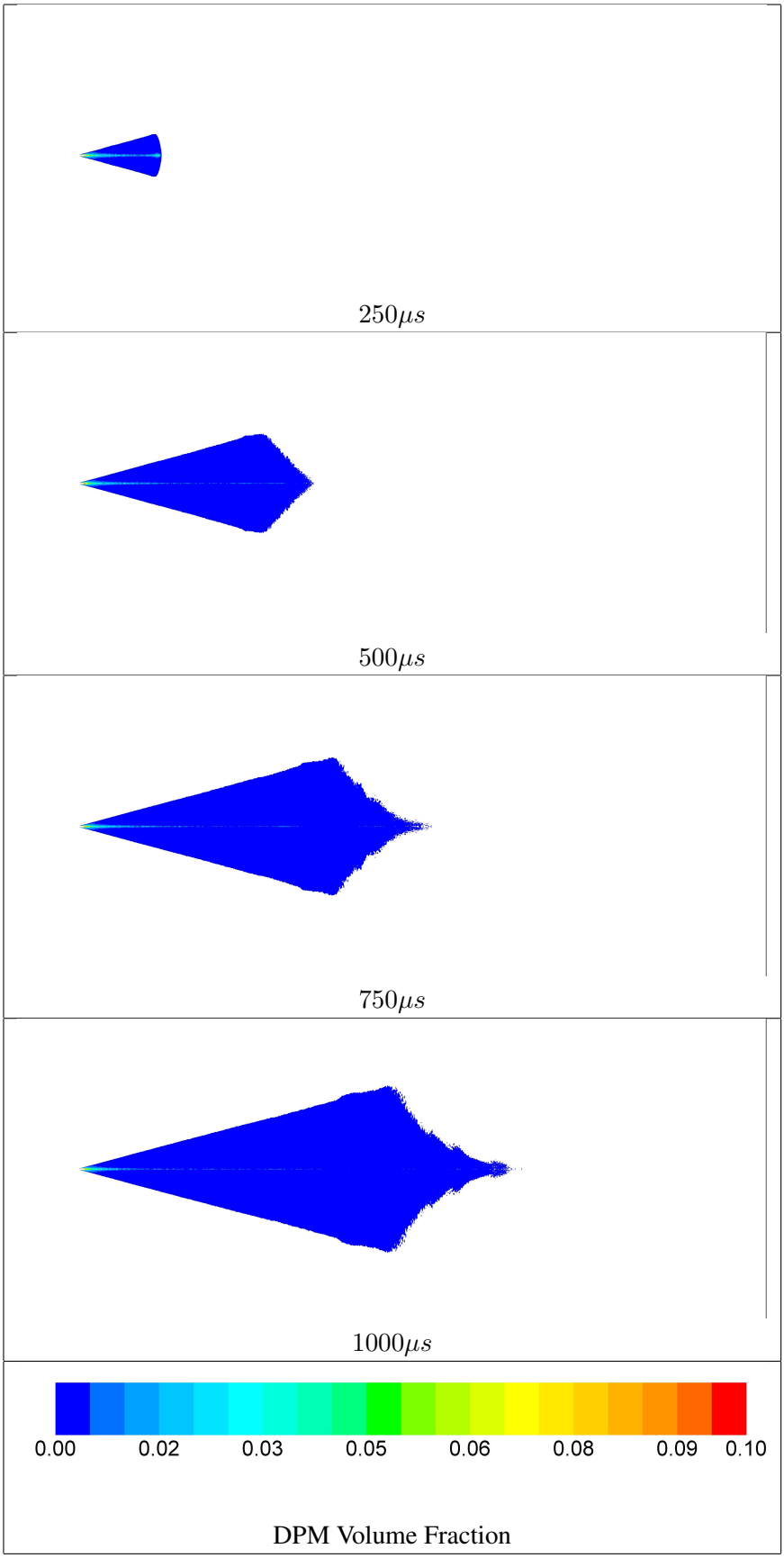

Figure 4.13. T=120 Pv=40 kPa

CHAPTER 5

CONCLUSIONS

5.1. Conclusions

The results shows that the ability of prediction changes depending on cases. The reasons why the model does not work in some cases whereas it works in other cases. From the general point of view, the number of parcels injected at each time step is 300 whereas some studies (Bianchi et al. (2001), Kösters and Karlsson (2011)) set this numbers as 12000. The computational and time cost are limited this number which differs significantly from the other studies. The more parcel number, the more statistical convergence and smoother source terms are provided. The coupling of both phases is any other issue. In this study the number of continuous phase iterations per DPM iteration is 10. As it is increased, time cost is needed.

Secondly, bad prediction could be attributed to the plain orifice atomizer model which is not used widely. This atomizer model evaluates the state of nozzle flow as flipped, cavitating and single phase alternately. This cause difficulties in convergence.

The other source of the problem is the grid resolution. Finer than necessary level of grid resolution could effect in a negative way. In some dense regions DPm volume fraction exceeds even more than 5 and it gives non-physical results in terms of exchange of liquid and gas phase.

To mention about effervescent atomizer, the spray angle tends to keep constant after a while whereas according to the experimental results the spray angle gets narrower. It overpredicted penetration at the temperatures of 363 and 393 K at 40 kPa chamber pressure (see Fig. 4.7, 4.8, 4.11). The model did not succeed at predicting either spray angle or penetration.

Fig. 4.3 depicts that the penetration results the case for Tf=293 K and Pv=101 kPa are predicted well whereas spray angle results agree with the experimental data after approximately 650 μs from the beginning of injection. Fig. 4.4 shows that the penetration results at 363 K fuel temperature at the concerning pressure are overpredicted between 50 and 200 μs and then predicted well. However,

For case Tf=20 at 101 bar pressure 50 ms after it exits the nozzle, it disperses while the case for Tf=90 keep more compact due to initial nozzle flow state. It vaporizes and losses some part of parcels and exchanges non-physically momentum with surrounding air. Fig. 5.1 shows the non-physically increasement in discrete phase velocity and then it creates a jump in spray penetration graphic (Fig. 4.4).

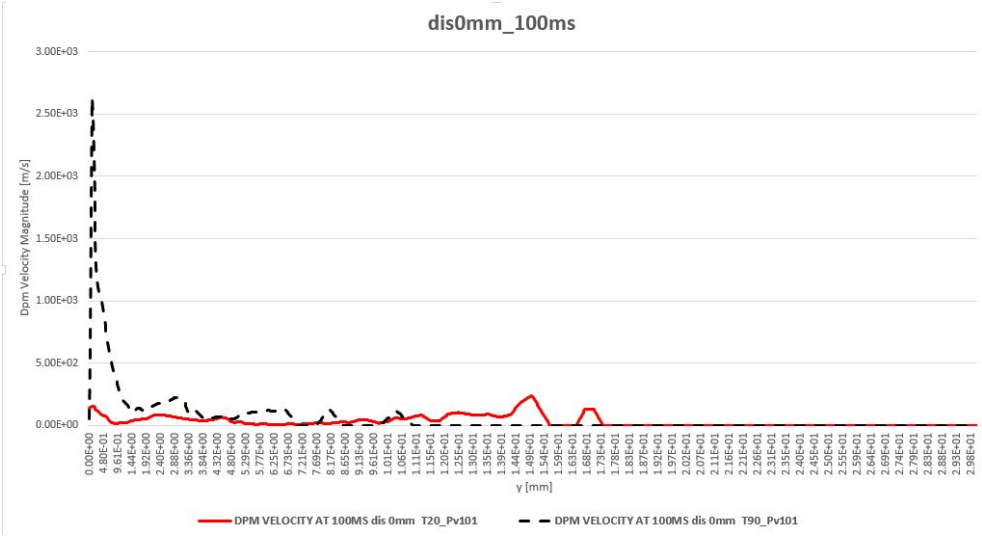

Figure 5.1. Discrete Phase Velocity Magnitude at nozzle at 100 μs

5.2. Future Work

Lagrangian-Eulerian method is strongly mesh-dependent. In contrast to this fact, regarding time-cost and violation of Lagrangian definition which void fraction must equal to almost one the grid sizes can not be reduced to the level that the Lagragian phase volume fraction exceeds 0.1. To avoid mesh-dependency some phenomenological models have been developed. These models are implemented into CFD codes. In present study CFD is not supported by an additional model. As a future work, the implementation of one of the following models is aimed.

Bekdemir et al. (2008) used the one-dimensional phenomenological spray model based on mass, momentum and energy balance within the control volume (see Fig. 5.2). But after solving three coupled equations derived from mass, momentum and energy conservation, he convert the steady velocity profiles into unsteady profiles. The aim was calculation of mass, momentum and energy sources and implementation them into FLUENT.

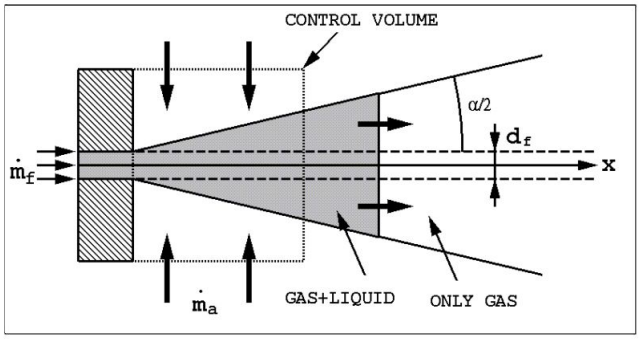

Figure 5.2. Phenomenological Spray Model (Versaevel et al. (2000))

To improve the model some improvements listed below could be done so that the model could be more grid-independent and work under all operating conditions:

- Grid resolution could be higher than enough level. Liquid volume fraction exceeds to even 5 in dense region during simulation.
- Fluent is hard to implement some phenomenological models. Hence, for future works more flexible and open source CFD software will be preferred rather than FLUENT.
- In plain orifice atomizer the flow state changes in time. It creates instability while simulation and convergence difficulties. Flipped, cavitating and single phase nozzle flows are given alternately, it does not converge at all. Instead of this atomizer model, phenomenological nozzle exit models need to be used.
- More parcels must be injected. Because the more parcel the more accuracy in statistical convergence and more smooth source terms are gained.
- The coefficient for k and epsilon model as in the study of Kösters and Karlsson (2011) and WAVE breakup model must be tuned.

  Bianchi et al. (2001) proposed an updated hybrid model to previous hybrid model.Bianchi and Pelloni (1999) that had been applied with success to an in-line pump injection systems to treat all injected blobs by the atomization model previously presented in this paper.
- Kösters and Karlsson (2011) implemented the correlation (Eq. 5.1 to limit the turbulent length scale to the nozzle diameter and applied all cells occupied by at least

one parcel. This is because the jet itself drives the flow (Stiesch, 2013).

$$\varepsilon = C_{\mu}^{3/4} \frac{k^{3/2}}{d_{nozzle}} \tag{5.1}$$

REFERENCES

Abani, N., S. Kokjohn, S. W. Park, M. Bergin, A. Munnannur, W. Ning, Y. Sun, and R. D. Reitz (2008). An improved spray model for reducing numerical parameter dependencies in diesel engine CFD simulations. *SAE Technical Paper 2008-01-0970*.

Abani, N., A. Munnannur, and R. D. Reitz (2008). Reduction of numerical parameter dependencies in diesel spray models. *130*.

Abraham, J. (1997). What is adequate resolution in the numerical computations of transient jets? Technical report, SAE Technical Paper.

Allocca, L., A. Montanaro, R. Di Gioia, and G. Bonandrini (2014). Spray characterization of a single-hole gasoline injector under flash boiling conditions. Technical report, SAE Technical Paper.

Arcoumanis, C., M. Gavaises, and B. French (1997). Effect of fuel injection processes on the structure of diesel sprays. Technical report, SAE Technical Paper.

Ashgriz, N. (2011). *Handbook of atomization and sprays: theory and applications*. Springer Science & Business Media.

Badami, M., F. Millo, and A. Pinzello (2008). The extended phenomenological spray model (epsm): A new approach for cfd diesel fuel spray simulation under evaporative and nonevaporative conditions. *Atomization and Sprays 18*(8).

Baumgarten, C. (2006). *Mixture formation in internal combustion engines*. Springer.

Beard, P., J.-M. Duclos, C. Habchi, G. Bruneaux, K. Mokaddem, and T. Baritaud (2000). Extension of lagrangian-eulerian spray modeling: Application to high pressure evaporating diesel sprays. Technical report, SAE Technical Paper.

Bekdemir, C., L. Somers, and L. de Goey (2008). Numerical modeling of diesel spray formation and combustion. *Eindhoven University of Technology, Netherlands*.

Bianchi, G., C. Forte, S. Negro, and P. Pelloni (2008). A 1d model for the prediction of flash atomization in gdi multi-hole injectors: preliminary results. *SAE International Journal of Engines 1*(2008-01-2516), 1278–1293.

Bianchi, G. and P. Pelloni (1999). Modeling the diesel fuel spray breakup by using a hybrid model. *Journal of Engineering for Gas Turbines and Power*.

Bianchi, G. M., P. Pelloni, F. E. Corcione, L. Allocca, and F. Luppino (2001). Modeling atomization of high-pressure diesel sprays. *Journal of Engineering for Gas Turbines and Power* (2).

Chehroudi, B., S.-H. Chen, F. V. Bracco, and Y. Onuma (1985). On the intact core of full-cone sprays. Technical report, SAE Technical Paper.

Desantes, J. M., R. Payri, F. J. Salvador, and J. Gimeno (2006). Prediction of spray penetration by means of spray momentum flux. Technical report, SAE Technical Paper.

Dukowicz, J. K. (1980). A particle-fluid numerical model for liquid sprays. *Journal of Computational Physics 35*(2), 229 – 253.

Fluent, A. (2009). 12.0 theory guide. *Ansys Inc 5*.

Froessling, N. (1938). Über die verdunstung fallender tropfen. *Gerlands Beiträge zur Geophysik 52*, 170–215.

Gonzalez D, M., Z. W. Lian, and R. Reitz (1992). Modeling diesel engine spray vaporization and combustion. *SAE transactions 101*(3), 1064–1076.

Hillier, V. A. W. and P. Coombes (2004). *Hillier's fundamentals of motor vehicle technology*. Nelson Thornes.

Hiroyasu, H. and M. Arai (1980). Fuel spray penetration and spray angle in diesel engines. *Trans. JSAE 21*(5), 11.

Hiroyasu, H. and M. Arai (1990). Structures of fuel sprays in diesel engines. Technical report, SAE Technical Paper.

Hiroyasu, H., M. Arai, and M. Tabata (1989). Empirical equations for the sauter mean diameter of a diesel spray. Technical report, SAE Technical Paper.

Horrocks, R. (2010). 1 - overview of high-speed direct injection diesel engines. In H. Zhao (Ed.), *Advanced Direct Injection Combustion Engine Technologies and Development*, Volume 2, pp. 3 – 60. Woodhead Publishing.

Huh, K. and A. Gosman (1991). A phenomenological model of diesel spray atomization. In *Proceedings of the international conference on multiphase flows*, Volume 91.

Johnson, K. G., K. Mollenhauer, and H. Tschöke (2010). *Handbook of diesel engines*. Springer Science & Business Media.

Kawano, D., Y. Goto, M. Odaka, and J. Senda (2004). Modeling atomization and vaporization processes of flash-boiling spray. Technical report, SAE Technical Paper.

Kösters, A. and A. Karlsson (2011). A comprehensive numerical study of diesel fuel spray formation with openfoam. Technical report, SAE Technical Paper.

Levich, V. G., S. Technica, et al. (1962). *Physicochemical hydrodynamics*, Volume 689. Prentice-hall Englewood Cliffs, NJ.

Liu, A. B., D. Mather, and R. D. Reitz (1993). Modeling the effects of drop drag and breakup on fuel sprays. Technical report, DTIC Document.

Moyne, L. (2010). Trends in atomization theory. *International Journal of Spray and Combustion Dynamics 2*(1), 49–84.

Nurick, W. (1976). Orifice cavitation and its effect on spray mixing. *Journal of fluids engineering 98*(4), 681–687.

O'Rourke, P. and A. Amsden (1987, Jan). *The tab method for numerical calculation of spray droplet breakup*.

O'Rourke, P. J. (1981). Collective drop effects on vaporizing liquid sprays. Technical report, Los Alamos National Lab., NM (USA).

Pickett, L., G. Bruneaux, and R. Payri (2014). Engine combustion network. *Sandia National Laboratories, Livermore, CA, http://www. ca. sandia. gov/ecn*.

Pickett, L. M., C. L. Genzale, J. Manin, L. Malbec, and L. Hermant (2011). Measurement uncertainty of liquid penetration in evaporating diesel sprays. *ILASS2011-111*.

Pope, S. (1978). An explanation of the turbulent round-jet/plane-jet anomaly. *AIAA journal 16*(3), 279–281.

Postrioti, L. and M. Battistoni (2010). Evaluation of diesel spray momentum flux in transient flow conditions. Technical report, SAE Technical Paper.

Postrioti, L., M. Battistoni, C. Ungaro, and A. Mariani (2011, April). Analysis of diesel spray momentum flux spatial distribution. *4*(1), 720–736.

Postrioti, L., M. Bosi, A. Cavicchi, F. AbuZahra, R. Di Gioia, and G. Bonandrini (2015). Momentum flux measurement on single-hole gdi injector under flash-boiling condition. Technical report, SAE Technical Paper.

Postrioti, L., F. Mariani, M. Battistoni, and A. Mariani (2009). Experimental and numerical evaluation of diesel spray momentum flux. Technical report, SAE Technical Paper.

Ranz, W. and W. Marshall (1952). Evaporation from drops. *Chem. Eng. Prog 48*(3), 141–146.

Ranz, W. E. (1958). Some experiments on orifice sprays. *The Canadian Journal of Chemical Engineering 36*(4), 175–181.

Reitz, R. and F. Bracco (1982). Mechanism of atomization of a liquid jet. *Physics of Fluids (1958-1988) 25*(10), 1730–1742.

Reitz, R. D. (1987). Modeling atomization processes in high-pressure vaporizing sprays. *Atomisation Spray Technology 3*, 309–337.

Reitz, R. D. (1990). A photographic study of flash-boiling atomization. *Aerosol Science*

and Technology 12(3), 561–569.

Reitz, R. D. and R. Diwakar (1987). Structure of high-pressure fuel sprays. Technical report, SAE Technical Paper.

Schmidt, D. P. and M. L. Corradini (1997). Analytical prediction of the exit flow of cavitating orifices. *Atomization and Sprays 7*(6).

Schmidt, D. P. and C. Rutland (2000). A new droplet collision algorithm. *Journal of Computational Physics 164*(1), 62–80.

Schmidt, D. P. and P. Senecal (2002). Improving the numerical accuracy of spray simulations. Technical report, SAE Technical Paper.

Soteriou, C., R. Andrews, and M. Smith (1995). Direct injection diesel sprays and the effect of cavitation and hydraulic flip on atomization. Technical report, SAE technical paper.

Stiesch, G. (2013). *Modeling engine spray and combustion processes*. Springer Science & Business Media.

Versaevel, P., P. Motte, and K. Wieser (2000). A new 3d model for vaporizing diesel sprays based on mixing-limited vaporization. Technical report, SAE Technical Paper.

Wan, Y. and N. Peters (1997). Application of the cross-sectional average method to calculations of the dense spray region in a diesel engine. Technical report, SAE Technical Paper.

Williams, F. (1958). Spray combustion and atomization. *Physics of Fluids (1958-1988) 1*(6), 541–545.

Wu, P.-K., L.-K. Tseng, and G. Faeth (1992). Primary breakup in gas/liquid mixing layers for turbulent liquids. *Atomization and Sprays 2*(3).

Xu, M., Y. Zhang, W. Zeng, G. Zhang, and M. Zhang (2013). Flash boiling: easy and better way to generate ideal sprays than the high injection pressure. Technical

report, SAE Technical Paper.

APPENDIX A

DISCRETE PHASE NUMERICAL SETUP

The option of steady or transient treatment is independent of the setting for the solver.However,when breakup or collision model is enabled ,automatically The transient particle tracking is switched on.In this case,the breakup of the droplets is taken into consideration.

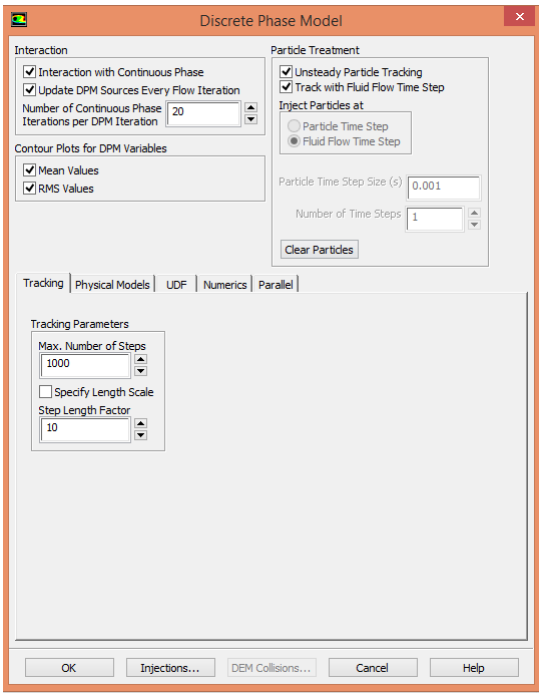

Figure A.1. Discrete Phase Dialog Box

If the discrete phase exchanges mass,momentum and/or energy with the continous phase,The **Number of Continous Phase Iterations per DPM Iteration** allows to control the frequency at which the particles are tracked and the DPM sources are updated.The **Update DPM sources every flow iteration** is must be enabled when doing unsteady simulations and at every DPM iteration the particle source terms are recalculated are applied to the continuous phase equations.

A.1. Tracking Parameters

Two parameters are defined to control the time integration of particle trajectory equations(Eq.**??**) (see The Fig.A.1)

- **The maximum number of time step**:is the maximum number of time steps used to compute a single particle trajectory.The simulation gets rid of the possibility for a particle being caught in a recirculating zone and being tracked infinitely.When the maximum number is exceeded,Fluent exit the trajectory calculation for the current particle injection and reports the trajectory fate as "incomplete".In this case this limit can be increased up to the limit of 10^9

- **The Length scale/Step Length Factor**:controls the integration time step size used to integrate the motion equations.

$$\Delta t = \frac{L}{u_p + u_c}, \tag{A.1}$$

where L is specified length scale,which proportional with time step size.

Step length factor defined in the Eq.A.2 as $\lambda$is used to control the time step size as well as The Length Scale does.However,The length scale,defined as Λ in the Eq.A.2 gives the number of time steps required for a particle to pass through a computational cell.Δt^* is an estimated transit time for a particle to traverse the current continous phase control volume.

$$\Delta t = \frac{\Delta t^*}{\lambda}, \tag{A.2}$$

If the particles are required to go towards a domain in which there are N mesh cells into the main flow direction,the **Step Length Factor** times N should be equal to **Max. Number of Step**.